IOP Publishing Journal of Physics B: Atomic, Molecular and Optical Physics
J. Phys. B: At. Mol. Opt. Phys. **50** (2017) 032001 (27pp) doi:10.1088/1361-6455/50/3/032001

Topical Review

Recent progress of below-threshold harmonic generation

Wei-Hao Xiong[1], Liang-You Peng[1,2] and Qihuang Gong[1,2]

[1] State Key Laboratory for Mesoscopic Physics and School of Physics, Peking University; Collaborative Innovation Center of Quantum Matter, Beijing 100871, People's Republic of China
[2] Collaborative Innovation Center of Extreme Optics, Shanxi University, Taiyuan, Shanxi 030006, People's Republic of China

E-mail: liangyou.peng@pku.edu.cn

Received 19 May 2015, revised 3 November 2016
Accepted for publication 9 November 2016
Published 13 January 2017

Abstract

The harmonics generated from the interaction of a strong laser field with atoms and molecules in the gas phase can be applied as coherent light sources and detecting techniques for structures and dynamics in matter. In the last three decades, the most prevailing experimental and theoretical studies have been focused on the high-order harmonic generation due to its applications in attosecond science. However, low-order harmonics near the ionization threshold of the target have been less explored, partially because the spectrum in this region is more complicated from both the theoretical and experimental point of view. After several pioneering investigations in the mid 1990s, near threshold harmonics (NTHs) begun to draw a great attention again because of the development of high repetition rate cavity enhanced harmonics about 10 years ago. Very recently, NTHs have attracted a lot of experimental and theoretical studies due to their potential applications as light sources and complicated mechanisms. In this topical review, we will summarize the progress of NTHs, including the early and recent experimental measurements in atoms and molecules, as well as the relevant theoretical explorations of these harmonics.

Keywords: near threshold harmonics, semiclassical methods, quantum path interference, resonance effects

(Some figures may appear in colour only in the online journal)

1. Introduction

The interaction of atoms and molecules with strong laser fields can lead to many interesting phenomena, such as above threshold ionization [1–3], high-order harmonic generation (HHG) [4, 5], multiple ionization [6], dissociative ionization and Coulomb explosion [7], and so on. These phenomena can reveal the electronic and nuclear dynamics as well as their correlation, which deepens our understandings of the underlying mechanisms for the internal dynamics under the manipulation of the strong laser field.

In particular, the process of HHG can not only serve as spectroscopic imaging tools but also provide us with coherent light sources in the extreme ultraviolet (XUV) range. On one hand, high-order harmonics have been applied as a table top light sources for those experiments which need large photon energies, e.g., excitation of the electronic states of molecules. On the other hand, the coherence of these harmonics allow us to generate laser pulses with durations as short as tens of attoseconds [8–10], which have pushed the investigations on the ultrafast dynamics from the femtosecond (10^{-15} s) to the attosecond (10^{-18} s) regime [11]. With the availability of these attosecond pulses and the protocol of attosecond streaking, an unprecedented time resolution has been achieved in observing and controlling many ultrafast dynamics inside atoms, molecules, and solids [11–14].

The investigation of HHG in the gas phase started from the discovery of plateau regime in the late 1980s [4, 5],

although a similar plateau structure was observed in the laser-plasma interaction context at an earlier time [15, 16]. In the very beginning when the laser intensity was weak, one thinks that the harmonic yield drops exponentially with the increase of the harmonic order due to the decreasing nonlinear susceptibility [17]. However, when the electric field strength of the driving pulse became stronger, after the fast drop in the yield of low-order harmonics, the experiments observed a long plateau, where the harmonic yield does not change much with the increase of the harmonic order. This plateau is followed by a sharp cutoff of the photon energy. These highly nonlinear phenomena suggest the inapplicability of the perturbation theory and a feasible way to synthesize a laser pulse in the sub-femtosecond domain based on the broadband spectra with comparable amplitudes [18–20].

After the discovery of the plateau in the harmonic generation, the major efforts in both the theoretical and the experimental studies have been focused on the tabletop XUV light sources and the generation of attosecond pulses [8–10, 21]. Essentially, through the manipulation of the driving laser pulses in one-color or multiple colors, the harmonic emission process can be effectively controlled to select certain harmonics, to enhance the harmonic conversion efficiency, to generate a broad supercontinuum, or to extend the cutoff energy. For example, with an optimization of a strong mid-infrared driving laser, the cutoff energy of high-order harmonics has been extended to the keV x-ray regime [22].

Unlike the prevailing investigations on the HHG for more than 30 years, the low-order harmonics below or near the ionization threshold of the target have attracted much less attention. Initially, these low-order harmonics were thought to be a perturbative response [17]. However, in the mid of 1990s, several experiments in the near threshold harmonics (NTHs) were carried out in an elliptically polarized field and an anomalous ellipticity dependence of the harmonic yield was observed [23–25], which was partially beyond the explanation of the strong field approximation (SFA) [26] that has been routinely used to interpret the HHG process.

Ten years later, the potential applications as high repetition light sources in the VUV range [27, 28] begun to arouse revival interests in studying the below- or near-threshold harmonics. When the harmonic generation process happens in a cavity, the repetition rate can be quite high and the intensity of the driving pulse is not very strong due to the reduction of setups for the chirp pulse amplification. Thus, the generated harmonics are mostly lying in the near-threshold regime. The applications of these harmonics require the knowledge about the coherence and other properties of these harmonics, which have recently been investigated in experiments. In 2009, by exposing Xe atoms in an intense 1070 nm driving pulse, Yost *et al* [29] observed the quantum path interference, shown as step structures in the yield of the below threshold harmonics as a function of the laser intensity. Soon after that, a negative group velocity dispersion was observed in another experiment in a scaled Keldysh system [30]. These two experimental observations clearly revealed the failure of the perturbation theory in this regime and suggested a classical trajectory behavior in the generation of the low-order harmonics. Later on, a detailed experimental investigation has been carried out for NTHs from aligned molecules [31], which distinguished different impacts for short and long trajectories. Very recently, a carrier envelope phase (CEP) dependence of NTHs was observed in a double optical gating (DOG) scheme with a very short (about 1.3 fs) linear polarization window of two circularly polarized lasers and its double frequency component [32]. In addition, the CEP dependence of the low-order harmonics has been applied to reveal the bound electron dynamics in another experimental investigation [33]. They used a short driving pulse to investigate the bound electron dynamics and revealed a time delay of the electron's response to the applied field. Other properties of the low-order harmonics has also been investigated in experiments, such as the spatial distribution [34], the wavelength range of the emitted harmonics [35], and so on. These investigations are necessary in order to set a good foundation for the practical application of low-order harmonics as a reliable light source.

Along with the above experimental work, theoretical studies have been flourishing in the past few years in order to understand the underlying mechanisms behind the rich phenomena. The accurate theoretical description of the harmonic generation process mainly relies on the numerical solution to the time-dependent Schrödinger equation (TDSE) [36], in which the harmonic spectra can be extracted by transforming the time-dependent acceleration of the electron according to the classical theory of radiation. With the help of SFA, a transparent understanding of electron motion can be achieved for high order harmonics. The underlying picture behind the SFA is similar to that of the simple man's model: between the ionization and the recombination process, the electron's dynamics is assumed to be only governed by the laser field. For the harmonics in the high-energy plateau regime, the harmonic spectra calculated through the SFA [37] showed excellent agreement with those computed by the numerical solution to the TDSE. Through some modification to the recombination dipole element, the quantitative rescattering theory can achieve better agreement for the lower part of the plateau [38–40]. However, these method cannot be directly applied to describe the NTHs. These difficulties had been encountered soon after the discovery of the simple man's model [41–43] when one tried to explain the experimental observation of the abnormal ellipticity dependence of low-order harmonics [23–25].

One usually thought that the low energy regime of harmonic generation can be explained by the perturbation theory and the high energy part can be described by a three-step model. After the early experiments mentioned above, one finds that it is difficult to give a solid theoretical description for the low-order harmonics. On one hand, the perturbation theory cannot be applied to these processes when the driving laser is sufficiently intense [44]. On the other hand, due to the important roles played by the Coulomb potential and the bound states in the NTHs [45], methods (such as SFA) which neglects the Coulomb potential cannot be directly used to describe the NTHs as well. The quantum path interference [29] has suggested some classical aspects in the generating process. Therefore, the concept of the quantum trajectory may

be modified to partially include the effect of the Coulomb potential to reveal some insights into the NTHs. Indeed, recent theoretical studies showed that the three-step model still can be applied in this regime to discuss the trajectories of electrons [46]. In the semi-classical description, the electrons are treated classically after the tunneling ionization, the Coulomb potential can be taken into account in the classical Newton's equation. It turned out that this kind of semi-classical description has helped us to get a better understanding for NTHs, although it is not quantitatively accurate. The classical description can be extended to the classical trajectory Monte Carlo (CTMC) model to calculate the low-order harmonic yields, which can have a rather good agreement with the TDSE results in the tunneling deep regime [47]. In addition, it was found that the classical simulations can also be compared to the time–frequency analysis of the TDSE results to shed light on the electron dynamics below or near the ionization potential [48, 49]. All these theoretical investigations have shown that both the quantum path interferences and the resonance effects can both greatly impact the NTHs.

The purpose of the present topical review is to give an account of the history and current status of the theoretical and experimental studies on the NTHs, presenting a consistent understanding of the rich phenomena. The rest of this paper is organized as follows: in section 2, we will sketch the theoretical concepts of harmonic generation. Since the details of these methods are basically the same as those for the calculation of HHG, we only introduce the concepts which are useful in understanding the experimental and theoretical results in NTHs. In section 3, we will survey the experimental results in NTHs, including those experiments in early years when an elliptically polarized driving pulse was applied. Then in section 4, we will review the theoretical progresses in the low-order harmonics, mainly focusing on the understandings of the underlying physics in atoms and molecules. At last, we will summarize in section 5.

2. Theoretical concepts of harmonic generation

In this section, we will introduce some theoretical methods and concepts for the harmonic generation process, including the numerical solution to the TDSE, the SFA, and the semi-classical models. The goal of this section is mainly to present a sketch of the relevant concepts with most of the details neglected.

The quantum mechanical description of the strong field phenomenon is based on the TDSE, to be numerically solved exactly or analytically with some approximations. If one defines $H_{\rm at} = -\frac{1}{2}\nabla^2 + V(\mathbf{r})$, the corresponding TDSE is then given by

$$\mathrm{i}\frac{\partial \Phi(\mathbf{r}, t)}{\partial t} = [H_{\rm at} + H_{\rm int}^{\rm L}]\Phi(\mathbf{r}, t), \qquad (1)$$

where the interaction Hamiltonian is expressed in the length gauge as: $H_{\rm int}^{\rm L} = -\mathbf{r}\cdot\mathbf{E}(t)$.

The numerical solution to the TDSE on the temporal and spatial grids can usually provide accurate results within the single active electron (SAE) approximation, but the computation cost is relatively large and the underlying physics is not transparent. Starting from the simple man's model, the CTMC method has been developed. The advantage of the CTMC is the effect of the Coulomb potential can be partially included in the electron's propagation after its tunneling ionization. Besides, several kinds of analytical solution to the TDSE have achieved much success along the line of the simple man's picture, among which the SFA is widely used due to its simplicity and transparent physical picture.

2.1. Numerical solution of TDSE

Here we only introduce the basic process of the numerical solution of TDSE, interested readers can find more details in a recent review [13] and references therein. To numerically solve the TDSE, one should first discretize the wave function in the space coordinates. The discretization scheme can be either even spaced (e.g., finite difference) or uneven spaced (e.g., finite element discrete variable representation). After the spatial discretization, one has to evolute the wave function in time, starting from the initial state (usually ground state) wave function. There are many methods for the time propagation of the wave function, such as the split-operator [50, 51] and the Arnoldi method [52]. In principle, once one has the time dependent wave function at any desired time instant, one can extract any physical observable.

In the numerical solution to the TDSE, the time-dependent wave function is usually calculated every time step during the whole interaction process of the atom with the laser field. Therefore, to get the harmonic spectrum, one can evaluate the expectation values of the acceleration of the electron as a function of time. Because of the Ehrenfest's theorem [36], the dipole acceleration can be written as

$$\mathbf{a}(t) = \langle \Phi(\mathbf{r}, t)| \; - \; \nabla V(\mathbf{r}) + \mathbf{E}(t)| \; \Phi(\mathbf{r}, t)\rangle, \qquad (2)$$

in which case one can assume the linearly polarized laser is along the z-axis. According to the classical theory of the electromagnetic radiation, one can obtain the harmonic spectrum from the power spectrum by making a Fourier transform of the time-dependent acceleration. One can also get some time information of the photon emission by some kind of time–frequency analysis [53–55].

2.2. Time frequency analysis for the emission time

The dipole acceleration is a time dependent function, the time–frequency analysis of this dipole acceleration can reveal the emission time of certain frequencies. The analysis can be a Gabor transform or a wavelet transform in the following form [53–55]:

$$\mathbf{A}(t_0, \Omega) = \int \mathbf{a}(t) W_{t_0,\Omega}(t) \mathrm{d}t, \qquad (3)$$

where $W_{t_0,\Omega}(t)$ is a window function, $|\mathbf{A}(t_0, \Omega)|^2$ indicates the intensity of harmonic whose energy is Ω and the emission time is t_0.

The power and reliability of the time–frequency analysis has been demonstrated by comparisons with the trajectories in

the semiclassical methods. The agreement between the time–frequency analysis from the TDSE and the semiclassical results is very good, especially for the cases of long wavelengths of the driving pulse [56]. Due to its success, the time–frequency analysis has recently been applied to interpret the low-order harmonics from a classical point of view [49].

2.3. Strong field approximation

The TDSE (1) can be solved analytically under the SFA. The SFA has made a lot of success in explaining both the ionized electron spectrum [2, 3] and the harmonic spectrum [37] in the high-energy plateau region. However, the SFA method can not be directly used to correctly describe the NTHs. Nevertheless, we will see that some mathematical and physical concepts from the SFA may still be borrowed into this low-energy region of the harmonics.

In the SFA method for the harmonic generation, one normally assumes that the excited states of atoms do not get involved in the electron ionization and photoemission process. At the same time, one assumes that the continuum states are not affected by the ionic potential and can thus be approximated by the Volkov states. In addition, the depletion of the ground state is ignored as well. Under these assumptions, the matrix element for the emission of a photon with a frequency of Ω in the harmonic process is given by [37]

$$M(\Omega) \sim -\int_{-\infty}^{\infty} \mathrm{d}t_1 \int_{-\infty}^{t_1} \mathrm{d}t_0 \int \mathrm{d}\mathbf{k} \exp\left[\mathrm{i}S_\Omega(t_1, t_0, \mathbf{k})\right] \times m(t_1, t_0, \mathbf{k}), \tag{4}$$

in which

$$m(t_1, t_0, \mathbf{k}) = \langle \Psi_0(t) | \, \mathbf{r} \, | \mathbf{k} + \mathbf{A}(t_1) \rangle \times \langle \mathbf{k} + \mathbf{A}(t_0) | \, \mathbf{r} \cdot \mathbf{E}(t_0) | \Psi_0(t_0) \rangle$$

and the phase term is explicitly written as

$$S_\Omega(t_1, t_0, \mathbf{k}) = \int_{t_1}^{\infty} \mathrm{d}\tau (I_\mathrm{p} - \Omega) - \frac{1}{2}\int_{t_0}^{t_1} \mathrm{d}\tau [\mathbf{k} + \mathbf{A}(\tau)]^2 + \int_{-\infty}^{t_0} \mathrm{d}\tau I_\mathrm{p}, \tag{5}$$

with I_p being the ionization potential of the target atom.

The physical content that equation (4) conveys is very clear: the electron makes a transition from the ground state directly to the continuum at some time t_0, then it propagates in the continuum with the presence of the laser field, until a later time t_1 when it returns to the range of the binding potential and recombines with the ionic core to emit a photon with a frequency Ω.

To get the photon emission transition amplitude, the computation effort is daunting if one tries to carry out the multiple integrations in equation (4). However, in most of the cases, the phase term (5) is usually a fast oscillating function, which makes it eligible to use the saddle point method to evaluate the integrations. It turns out that the saddle point method is endowed with an intuitive picture of quantum orbits [57, 58]. In the saddle point approximation, the transition amplitude equation (4) recasts in the form of a sum over all the saddle points as follows

$$M = \sum_n a_n \mathrm{e}^{\mathrm{i}S_\Omega(t_n^\mathrm{s})}, \tag{6}$$

where a_n is an amplitude and t_n^s is determined by a set of saddle point equations, which turns out to be complex since $I_\mathrm{p} > 0$. The real part of t_n^s is referred to the time when the electron reaches the tunnel exit. To be specific, the saddle points for the harmonic process are given by the solutions to the following equations:

$$[\mathbf{k} + \mathbf{A}(t_0)]^2 = -2I_\mathrm{p}, \tag{7}$$

$$(t_1 - t_0)\mathbf{k} = -\int_{t_0}^{t_1} \mathrm{d}\tau A(\tau), \tag{8}$$

$$[\mathbf{k} + \mathbf{A}(t_1)]^2 = 2(\Omega + I_\mathrm{p}). \tag{9}$$

The above conditions physically means in turn the energy conservation in the process of tunneling, the condition that the electron returns to the ionization position, and the generation of a harmonic photon with energy Ω by its recombination with the core.

The saddle points t_n^s define a class of quantum orbits, in which the electron departs from the ionic core and returns to the ionization point to recombine. Actually, the real parts of these orbits are very closely related to the trajectories in the simple man's model and the imaginary part of the ionization time is related to the probability of the corresponding trajectory. The concept of quantum orbits establishes a bridge between the quantum and the classical mechanics. In the high photon energy regime, the ionization and recombination times for different photon energies can be compared with those extracted by the time–frequency analysis of the time-dependent acceleration, as shown in equation (3).

The final harmonic spectrum from the SFA can be expressed as coherent superpositions of contributions by different trajectories. For instance, if one considers a simplified situation of equation (6) where only two shortest trajectories are considered, then the transition matrix of the photoemission is given by

$$M(\Omega) = a_1 \exp(S_1) + a_2 \exp(S_2). \tag{10}$$

The final harmonic yield is modulated by the phase of the contributing trajectories. Thus if one calculates the harmonic yield in different laser parameters and examines the harmonic yield $|M(\Omega)|^2$ with a fixed Ω, one can observe the interference structure contributed by different trajectories. This had been observed just when the SFA was first proposed [37]. With the change of the laser intensity, the phase difference between S_1 and S_2 changes accordingly. This kind of interference structure have been verified by both the TDSE calculations and the experimental measurements [59].

2.4. Simple man's model and CTMC

In the simple man's model [41–43], the strong-field ionization process is divided into several steps. In the first step, the electron enters the continuum by the optical field ionization through the distorted Coulomb potential suppressed by the laser electric field. Once the electron appears at the tunnel

exit (which is usually small and thus ignored in the simple man's model), the laser field will dominate the interaction and drive the electron away from the ionic core. At the last step, the electron can return to the core when the driving field reverses its direction. If the electron recombines to the ionic core, it can emit a photon with energy $\Omega = E_k + I_p$, where E_k is the kinetic energy of free electron at the return and I_p is the ionization potential of the atom. For the ionized electrons, only a fraction of them can return to the core and the maximum energy of the returning electrons is $3.17U_p$, where $U_p = I_0^2/4\omega^2$ is the pondermotive energy with I_0 being the driving laser intensity and ω the driving laser frequency. This maximum electron energy leads to a cutoff position in the harmonic spectrum at $\Omega = 3.17U_p + I_p$.

The simple man's model cannot provide more insights for the harmonic generation than the SFA. However, the advantage of this model is that the simplicity and the separated steps which allow one to accommodate the Coulomb potential in the propagation step. The modified model, including the impact of the Coulomb potential, can be used to qualitatively describe the low-order harmonics. If one considers the Coulomb potential in the propagation step, the final photon energy can be written as

$$\Omega = E_k + I_p + V(\mathbf{r}). \tag{11}$$

The photon energy Ω can be less than I_p if E_k is small enough since $V(\mathbf{r})$ is always negative [46].

Based on the above discussions, one can go one step further to simulate the harmonic generation process using the CTMC method, which has been successfully applied to discuss many strong field phenomena [60–65]. The CTMC method simulates all possible electron trajectories with different initial conditions and accumulates their contributions in the final harmonic yield. Specifically, an ensemble of electrons are initialized, each of whose probability is weighted by a quasi-static ionization rate at its ionization time [66]:

$$W(t_0, v_\perp^i) = W_0(t_0) W_1(v_\perp^i), \tag{12}$$

in which

$$W_0(t_0) \propto \left| \frac{(2I_p)^2}{E(t_0)} \right|^{2/\sqrt{2I_p}-1} \exp\left[-\frac{2(2I_p)^{3/2}}{|E(t_0)|} \right] \tag{13}$$

determines the ionization rate with respect to the tunneling time t_0 and

$$W_1(v_\perp^i) \propto \frac{\sqrt{2I_p}}{|E(t_0)|} \exp\left[\frac{\sqrt{2I_p}\,(v_\perp^i)^2}{|E(t_0)|} \right] \tag{14}$$

gives the initial lateral momentum distribution, where $E(t_0)$ is the laser electric field, $v_\perp^i$ is the randomly sampled initial transverse momentum. It should be noted that the probability $W(t_0, v_\perp^i)$ here is not the analytical rate for both t_0 and $v_\perp^i$. It is an intuitive combination of the ionization rate at t_0 from the ADK theory and the normalized initial lateral momentum distribution [64].

After the preparation of the initial conditions, these electrons are propagated according to the Newton's equation in the combined field of the laser pulse and the ionic potential. When the electron travels close enough to the core, one assumes that this electron recombines and at the same time a photon is recorded in the harmonic spectra. The corresponding photon energy is the summation of the potential energy and the electron's kinetic energy. After the end of the laser pulse, the final harmonic spectra is calculated by counting the number of photons in each photon energy bin.

One should be careful about the description of the recombination process in this model because the quantum recombination process does not have a classical correspondence. The most simplest choice is to judge the distance of the electron to the core, one assumes the recombination happens once it is smaller than a certain prescribed value. An alternative choice is to choose the recombination distance to be the electron's initial tunneling point [47], which is different for different trajectories depending on the ionization time. Xiong and coworkers [47] have compared the harmonic spectrum calculated by this choice to the results calculated by the simplest choice of the recombination distance at various fixed distances from 1 a.u. to 6 a.u. They found that the calculated harmonic spectra are essentially the same for different recombination distances. However, for the choice of fixed distances, the short trajectories corresponding to the ionization when the electric field is small can not be correctly described because the electrons are ionized quite far away from the core for these trajectories and the electric field reverses its direction immediately after the ionization: these electrons have a long distance to be accelerated toward the core and get a high energy when it recombines, which is actually incorrect as the electron energy should be small. Of course, in practice, these trajectories do not affect the harmonic spectrum very much since the ionization rate of these trajectories are extremely small and cannot be directly observed in the final spectrum [47]. The studies in [47] showed that the alternative choice of the tunneling exit as the recombination distance can avoid this problem and get a better description of these trajectories since in this case those electrons will recombine soon after their ionization.

3. Experimental observations in NTHs

As mentioned in the introduction, most of the investigations on the harmonic generation were focused on the plateau regime due to their promising applications as spectroscopic imaging tools and as ways of generating attosecond pulses. Therefore, the seemingly *useless* NTHs had been paid much less attention. On the other hand, the experimental observations for NTHs were also restricted by both the driving field and the photo-detection technology. In this section, we will first review the early experimental results and its possible explanation in low-order harmonics and then go to the more recent experimental measurements.

In the early 1990s, low-order harmonics were experimentally studied for an elliptically polarized driving pulse with different ellipticities [23–25]. At that time, the three-step model for the harmonic generation was just proposed, which

was faithfully used to interpret the high-order harmonics in the tunnelling regime. However, when used to predict the ellipticity dependence of lower-order harmonic yield, the three-step model gave a theoretical result which was different from that measured experimentally. On the contrary, the experimental and theoretical results coincided with each other for the high-order harmonics.

A few years ago, much attention began to go back to low-order harmonics due to the high repetition light source. Many novel phenomena have been experimentally observed and added our understanding to the NTHs, which have paved the way for applications of these harmonics as a coherent light source and a frequency comb both in the VUV regime [27–30]. In addition, one can generate a very short driving field with a wide range of frequency with a well controllable CEP stabilized for a long time and one can detect the phase of the emitted harmonics [32, 33]. Along with these studies, some other properties of these low-order harmonics have been experimentally explored [34, 35, 67, 68].

3.1. Ellipticity dependence of low-order harmonics in atoms and molecules

In 1993, the simple man's model was proposed, which was subsequently used to successfully explain many strong field phenomena. The simple man's model has become one of the powerful models in strong field physics, which can provide an institutive picture. There are two features in the HHG which can be predicted by the simple man's model: the cutoff energy and the ellipticity dependence of harmonic yield. The former has been introduced in the previous section, here we mainly focus on the prediction of the rapid drop of the harmonic yield with the increase of the driving laser ellipticity.

In the simple man's model, it requires the ionized electron return to the core to emit harmonics. For an elliptically polarized pulse, the electron will return to the core with a momentum drift in the perpendicular direction of the major axis. The recombination process requires the overlap between the returning continuum wavepackets and the ground state wave function. When the ellipticity is relatively small, there may be a significant overlap due to the spread of the continuum wavepackets. When the ellipticity becomes large, the momentum drift gets large as well and the returning electron may miss the ionic core. Therefore, the recombination probability as well as the harmonic yield decreases with the increase of the ellipticity of the driving field. This feature was experimentally verified at that time for the high-order harmonics [23–25].

However, for the low-order harmonics near the threshold, as we will see below, the early and recent experiments have shown that the ellipticity dependence becomes much more complicated in atoms and molecules, which is beyond the intuitive explanation of the simple man's model.

3.1.1. Early studies of ellipticity dependence for atoms. In the 1990s, the amplified Ti:sapphire lasers were used in most of the experiments to generate harmonics. For these laser parameters adopted, the atomic ionization happens in the tunneling regime, in which case the simple man's model works rather well for the qualitative understanding of the HHG. Many experiments were carried out to detect the HHG yield of different atomic species at various driving laser parameters. For an elliptically polarized pulse, these observations showed that the yield in high-order harmonics decreases when the ellipticity of the driving laser increases, as the simple man's model predicts. However, for several kinds of atoms, the experimental observations showed that the yield of low-order harmonics did not drop smoothly as the ellipticity increases.

In 1995, Burnett *et al* [23] reported the observation of the ellipticity dependence of harmonic generation of neon for a 754 nm laser at an intensity of 3×10^{15} W cm^{-2}. They found that the 13th harmonic ($\hbar\Omega \approx I_p = 21.56$ eV) has a peak around $\epsilon = 0.1$ when ϵ changes. The maximum harmonic yield is increased by 5 times compared with the harmonic yield at $\epsilon = 0$. This observation cannot be explained by the simple man's model and indicates some other mechanisms for the harmonics near the ionization potential. They also claimed that qualitatively similar behavior for the 13th harmonic yield was also observed for helium ($I_p \approx 24.59$ eV).

Several months later in the same year, Miyazaki and Takada [24] experimentally investigated this problem as well. The laser conditions of their investigation were similar to those used in [23]. They also observed a peak when change the value of ϵ for the 13th harmonic of neon. They found that the 13th order increases with an increasing ϵ and reaches the peak at $\epsilon = 0.3$–0.4. However, they never observed such an anomalous ϵ-dependence in helium, which was different from the measurement in [23]. Based on their observations, they attributed the observed differences to the different energy structures of these two atomic species. Two years later, they further performed another investigation on this topic in 1997 [25], which included a systematic measurement of ellipticity dependent harmonic for four different atomic species, i.e., He, Ne, Ar, and Kr. The experimental results of the ellipticity dependence of harmonic yield in different atoms were reproduced in figure 1. As one can see, the yield of low-order harmonics drops slower than the high-order harmonics. In particular, for some harmonic orders, the harmonic yield from an elliptically polarized driving field can be significantly larger than that in a linearly polarized field. The anomalous ellipticity dependence can be observed at the 11th and 13th harmonic for Ne and at the 7th and 9th harmonic for Ar and Kr respectively. Besides, their experimental results also showed that the harmonic yield measurement can also be affected by the sensitivity of the detection in different polarization direction. Since the detection has a higher sensitivity for vertically polarized field, the phenomenon can only be observed when the linear polarization starts from the horizontally polarized case ($\epsilon = 0$ corresponding to the horizontally polarized fundamental field). In this experiment, they did not observe the anomalous phenomenon in He as well. To explain this anomalous phenomenon, they suggested the phenomenon should be explained through the near resonant multiwave mixing process presented in an earlier investigation [69].

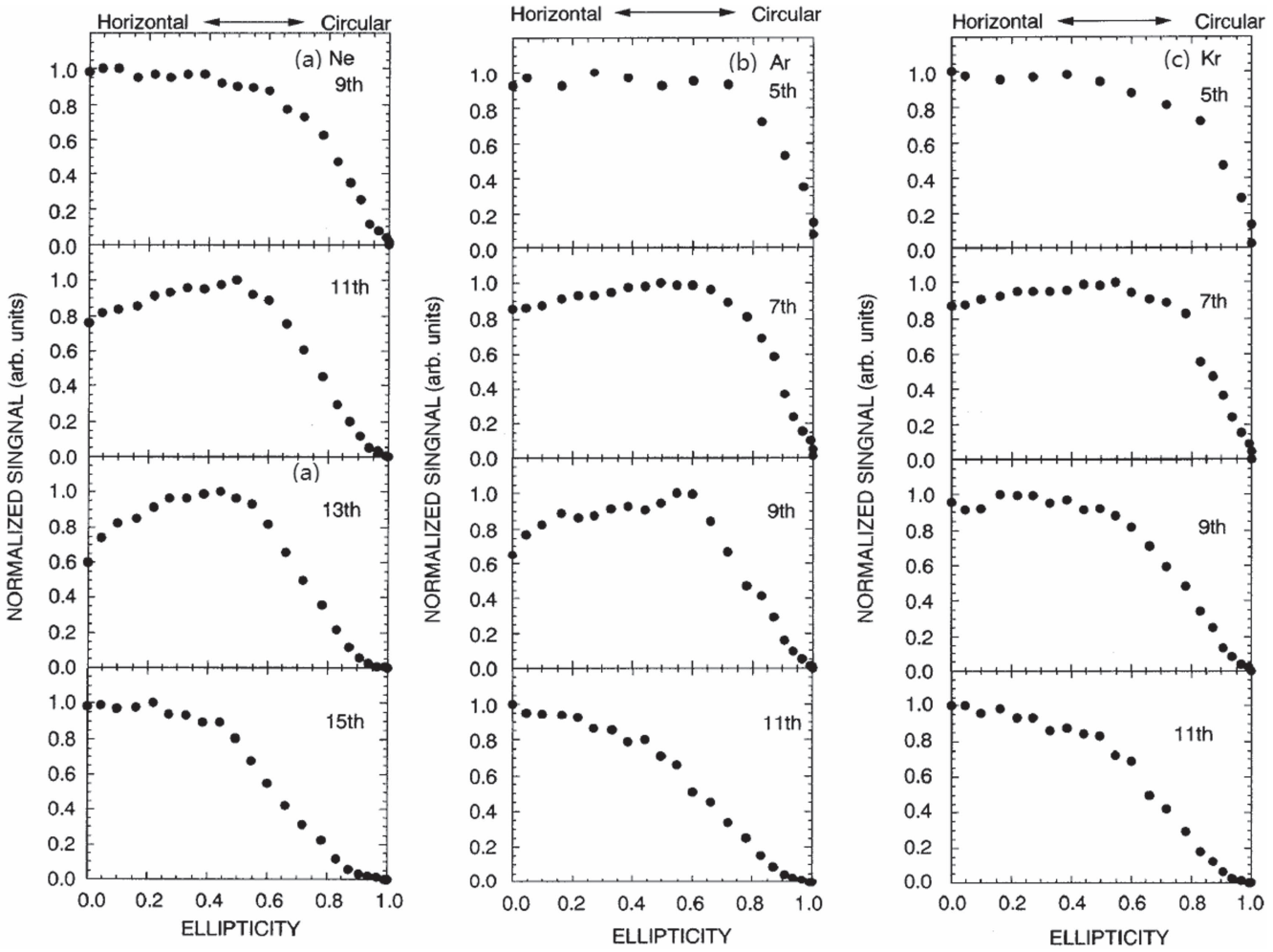

Figure 1. The ellipticity dependence of near threshold harmonics, measured for different atomic species: (a) Ne, (b) Ar, and (c) Kr. The driving field was a 785 nm Ti:sapphire laser at the maximum laser intensity around 3×10^{15} W cm^{-2} with a pulse duration about 150 fs. Reprinted figure with permission from [25]. Copyright 1997 by the American Physical Society.

In the 1990s, the theoretical interpretation of the HHG relied on the perturbation theory, the simple man's model, or the SFA. The perturbation theory is more applicable in the multiphoton regime and the simple man's model or the SFA works in the tunneling regime. The theoretical understanding of the ellipticity dependence of the low-order harmonics lies in taking the Coulomb potential into consideration within in the theoretical framework. However, the accurate consideration of the Coulomb potential in an analytical form is very difficult and remains a challenge. Nevertheless, one year after the experimental observation in [23], Ivanov *et al* [26] performed a theoretical investigation on this topic. They applied a quasiclassical approach to correct the electron's motion after the tunneling ionization in intense laser fields, in the presence of the Coulomb potential. Their calculations were in quite good agreement with experimental data in [23]. They offered a very intuitive explanation of the underlying physical picture as the theoretical method is trajectory based. They explained the different ellipticity behavior for the 13th and 15th harmonic results as an interference effect. Their theory has a transparently classical picture: the low order harmonics are generated by electrons born close to the peak of the electric field, which return to the parent ion with a low kinetic energy. For those electrons, the sign of the electron momentum and of the dipole moment is reversed during the second return. The superposition of the first and the second return leads to a destructive interference of the dipole moment. The destructive interference can cause a suppression of harmonic emission in the direction parallel to the main axis of the laser field. Hence, for a pulse with small ellipticity, the perpendicular component can dominate the harmonic emission and result in an increase of the total harmonic yield. In fact, this kind of descriptions in classical trajectories has been confirmed in recent investigations [29, 46] for linearly polarized lasers. However, there was no further study on the phase of these trajectories and their interference in the ellipticity dependence situation.

To our knowledge, there is no more work on the ellipticity dependence of the low-order harmonics in atoms after the above investigations. However, one cannot definitely conclude which explanation is the preferable one. The major difference between the experiments in the two groups is whether the abnormal phenomenon can be observed in helium. If this phenomenon cannot be observed in helium,

one wonders why the interference mechanism cannot explain the atomic species dependence. It seems that both the interference and the resonance mechanism play important roles in the NTH generation, which has been verified by recent investigations [45]. These two mechanisms can both influence the harmonic yield in some specific situations. Recently, the anomalous ellipticity dependence of harmonic yield has also been observed in aligned molecules [31], which will be briefly covered next.

3.1.2. Ellipticity dependence of NTHs in aligned molecules.

The investigation about the harmonic generation in the elliptically polarized laser fields has continued every since the mid 1990s, but most of the studied were focused on the high-order harmonics. The ellipticity dependence of the HHG usually has a Gaussian distribution, whose width is related to the electric field strength at the ionization time of the corresponding harmonic order.

Another interesting topic has been the ellipticity dependence of the harmonic yield in aligned molecules. For randomly oriented molecules, the overall harmonic generation spectra appear essentially the same as that in atoms. However, for aligned molecules, the asymmetry and multi-center interferences in the HHG of molecules can be observed [70–74]. If one takes the simplest molecule H_2^+ as an example, the returning electron can recombine to either of the two nuclear cores. The interference of these two paths can be observed in the harmonic spectrum which is a landmark feature for the HHG in aligned molecules. This kind of destructive interferences can lead to a similar abnormal phenomenon of the ellipticity dependence of the yield of HHG [75].

Things become more complicated when it comes to NTHs in molecules. Recently, under the interaction of elliptically polarized pulses with molecules (N_2 and O_2) [31], the anomalous ellipticity dependence is again observed in NTHs. Their results showed the ellipticity dependence is is related to both the molecular species and the molecular alignment. They identified two contributions of the harmonic signal near the ionization threshold through a classical electron trajectory analysis.

Their experimental results for O_2 are reproduced in figure 2, which shows the measured harmonic signal as a function of the laser ellipticity. Different alignment angles of 0° and 90° are shown in the left and right panel respectively. With the increase of the laser ellipticity, the harmonic yields for all the long trajectories (bottom panels) decrease smoothly, which agrees with the results of the simple man's model. But for the short trajectories, the abnormal ellipticity dependence can be observed (upper panels) in some situation. When the alignment angle is 0°, the yield of the 9th and 11th harmonics of O_2 increases as a function of the ellipticity and reaches a maximum when the ellipticity is around 0.2 and 0.15 respectively. A similar effect can be observed for an alignment angle of 90°, but only for the 9th harmonic. For harmonics above the ionization threshold, all the short and long trajectories are observed with a smooth decay.

They also performed experiments for N_2 molecules, the yield of all harmonic orders decreases smoothly with an

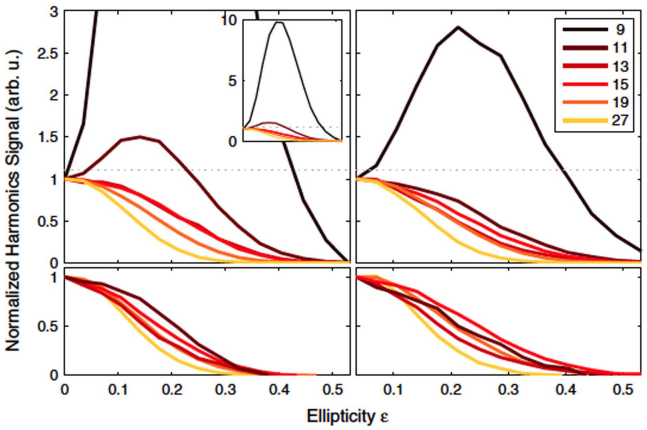

Figure 2. The experimentally measured ellipticity dependence of harmonic yields (with orders indicated) for the molecule O_2, at the molecular alignment angle 0° (left) and 90° (right). The contributions from the short and the long trajectories were shown in the top and bottom panel respectively. The driving field was an 800 nm laser with a peak intensity of 1.5×10^{14} W cm^{-2} and a duration of 30 fs. Reprinted figure with permission from [31]. Copyright 2010 by the American Physical Society.

increasing laser ellipticity for both the short and the long trajectories. Therefore, their results showed that all long trajectories follow the expected ellipticity dependence as predicted by the three-step model, while the responses of near-threshold short trajectories depend on the molecular species. Thus the observed enhancements for O_2 is not caused by the ground molecular orbital since its orbital is similar to that of N_2. Besides, these observations also cannot be related to the interference processes at the time of recombination [75], because this mechanism would affect both the short and long trajectories. For the long trajectories, they performed classical trajectory simulations and identified the electron's motion after its ionization.

In their studies, they observed two kinds of effects in NTHs. The long electron trajectories belong to the three-step model and encode the structural information in the same way as in the conventional high harmonic spectroscopy. The ellipticity dependence of these trajectories is the same as predicted by the simple man's model, which is not dependent on species. They also suggested that the short trajectories are generated from multiphoton-driven pathways, and can be used to reveal information about the excited states of the molecule. The observations in short trajectories may be related to the anomalous ellipticity dependency observed earlier in atoms, and the phenomenon is different for N_2 and O_2. After this experiment, some theoretical investigations were performed on the topic of the ellipticity dependence of molecular harmonic yield. These investigations verified the multiphoton-driven pathways and we will cover these works later.

3.2. Interference structures and negative group velocity dispersion in BTHs

In 2005, the experimental investigations on the low-order harmonics begun to attract revival interest, partially due to the

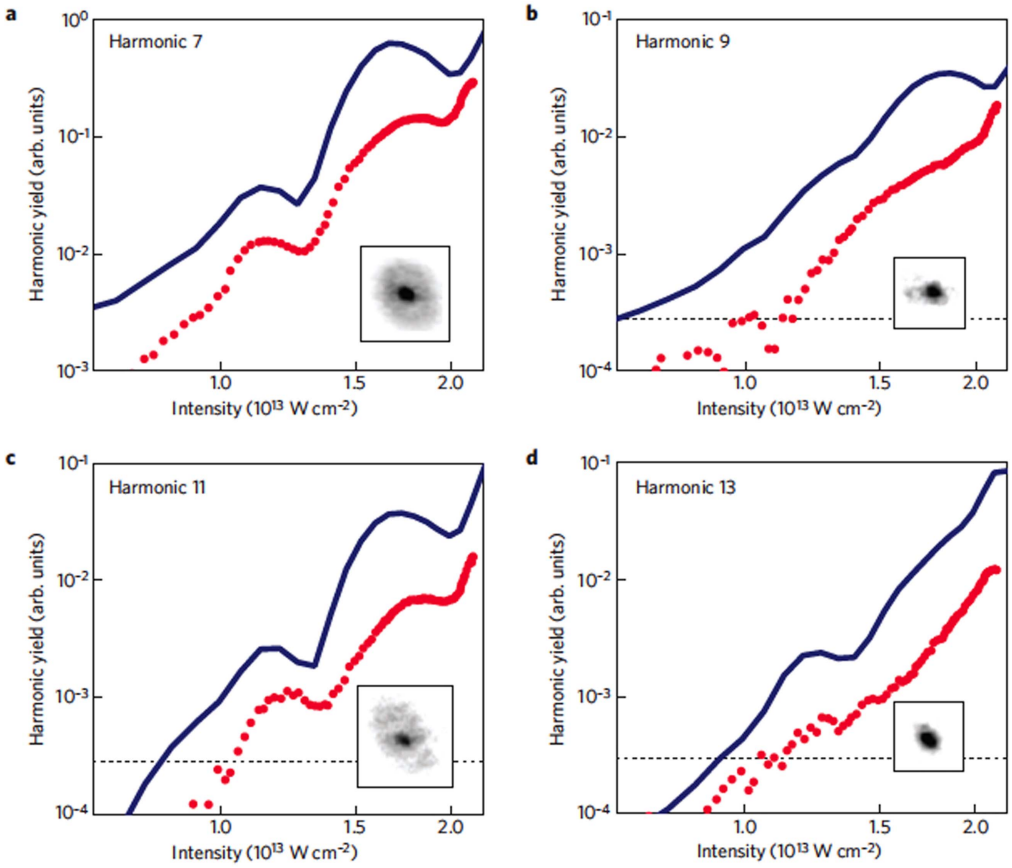

Figure 3. The yields of different orders of near threshold harmonics for Xe as a function of the peak intensity of a driven pulse at 1070 nm. The step and dip structures, clearly observable for the 7th, 11th, and 13th order, were caused by the quantum path interferences. The scaled TDSE results (solid lines) are in great agreement with those of the experimental data (red filled circles). Reprinted by permission from Macmillan Publishers Ltd: [29], copyright 2009.

development of cavity enhanced harmonic generation [27]. In the cavity setup, the low-order harmonics in the VUV range can be generated with a high repetition rate. The intra-cavity high harmonic generation were demonstrated in the XUV, which promises to lead to another joint frontier of the precision spectroscopy and the ultrafast science. With a cavity to enhance the driving laser, the chirp pulse amplification system is not necessary for generation of harmonics. This not only reduces the complexity of the setup for the generation of high harmonics compared to a typical chirped pulse amplification system but also increases the repetition rate of harmonic conversion by several orders of magnitude, reaching more than 100 MHz. At such a high repetition rate, the frequency comb from the fundamental laser will also be usable in the VUV regime, so that the high resolution spectroscopy in the VUV is available for various potential applications.

The generation of cavity enhanced harmonic generation not only leads to the frequency comb in the VUV range, but also draws much attention about the generation process itself, i.e., low-order harmonic generation, whose theoretical description is still unclear. The experimental investigation revealed the coherence [29, 30], the CEP dependence [32, 33], and some other properties of these harmonics [34, 35, 67, 68]. In this subsection, we will review these progresses and mainly focus on some of the representative experiments.

In 2008, Yost *et al* [29] noticed the lack of understandings for low-order harmonics and performed an experimental investigation on this topic. They presented a quantitative study of the harmonics generated below and near the ionization threshold in xenon gas with an intense 1070 nm driving field. In the experiment, they measured the harmonic yield as a function of the peak intensity of the driving laser, as shown in figure 3. As we can see, there are interference structures for the 7th, 11th, and 13th harmonics, while they are not obvious for the 9th order. This kind of interference structure as a function of the laser intensity in the high-order harmonics has been explained by the quantum path interference. Specifically, there are normally several quantum trajectories contributing to a certain harmonic order, and the phase of those trajectories changes with the laser intensity. The superposition of these trajectories then leads to the interference structures at different intensities. This phenomenon is similar to the intensity dependent structure in the HHG as predicted by the SFA [37] which has been verified by the experiment in 2008 [59].

The experimental observation of the interference structure indicates that the concept of trajectories in the simple

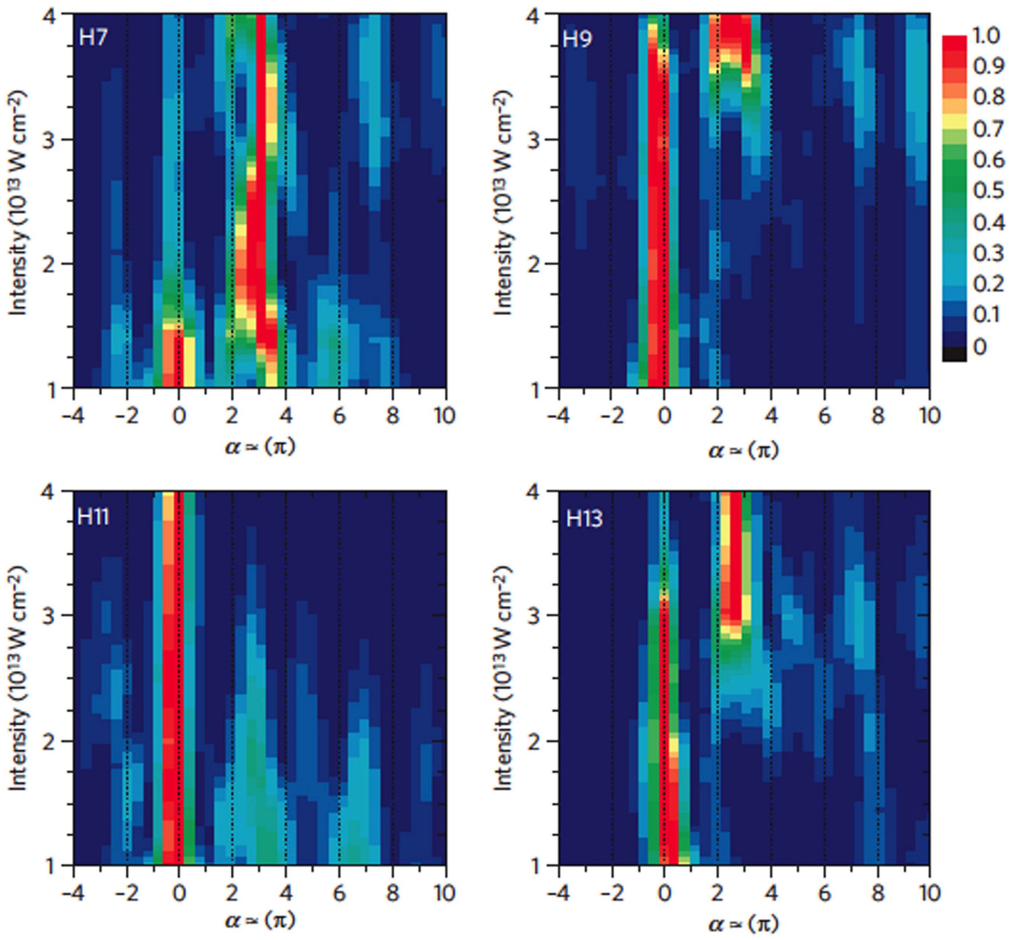

Figure 4. Theoretical quantum path distributions as a function of the laser peak intensity, calculated for harmonics from the 7th to the 13th. The color scale has been normalized for each intensity and shows only relative strengths. Reprinted by permission from Macmillan Publishers Ltd: [29], copyright 2009.

man's model is still applicable for the description of BTH generation. To explore the contributions by different quantum paths, they analyzed the single-atom intensity dependent dipole moment for each harmonic order in terms of its phase through a transform:

$$d_q(\alpha, I_0) = \int d_q(I) \mathrm{e}^{\mathrm{i}\alpha U_\mathrm{p}(I)/\hbar\omega} W(I - I_0) \mathrm{d}I, \qquad (15)$$

where I_0 and I is the laser intensity, $W(I - I_0)$ is a window function, and $d_q(I)$ is the qth harmonic yield when the driving laser intensity is I. The results can be interpreted using the equation (10) where the phase $S = \alpha U_\mathrm{p}(I)/\hbar\omega$. The calculated $d_q(\alpha, I_0)$ stands for the contribution of different trajectory phases α (or S) at the laser intensity of I_0. From the simple man's model, the two shortest trajectories are the usual short trajectory and the long trajectory. Their corresponding phases are $\alpha_1 \approx 0.2\pi$ and $\alpha_1 \approx 2\pi$ respectively.

Their theoretical results for NTHs are reproduced in figure 4 from 7th to 13th harmonic. As one can see, all of the harmonics show multiple quantum path contributions and the two dominant ones have phase coefficients $\alpha_1 \approx 0$ and $\alpha_1 \approx 2.5\pi$–3π. These calculations indicate that the concept of quantum path can be extended to the low energy range: there are short trajectories and long trajectories contributing to the NTHs. Usually, the short trajectories indicate a multiphoton excitation and recombination process while the long trajectories can be described by the inclusion of the Coulomb potential in the simple man's model. We will come back to the detailed theoretical interpretation of this kind of interference structure in the section 4.

Soon after the above work in [29], Power *et al* [30] characterized the phase of NTHs in a Keldysh scaled system, in which they observed a negative group velocity dispersion in these harmonics. Their observations were explained as the effects of long trajectories as well. Due to the limitation of the characterization techniques, they chose a Keldysh scaled system to measure the BTHs. Specifically, a mid-infrared laser at 3600 nm was used to produce harmonics from Caesium atoms. The resultant BTH harmonics simultaneously lies in the visible wavelength range and can be easily detected. In their experiments, the authors were able to measure the spectral amplitude and phase to reconstruct the harmonics. They performed the temporal characterization of BTHs using the sum frequency generation cross-correlation frequency resolved optical gating, a technique sensitive to the relative delay between different harmonic orders.

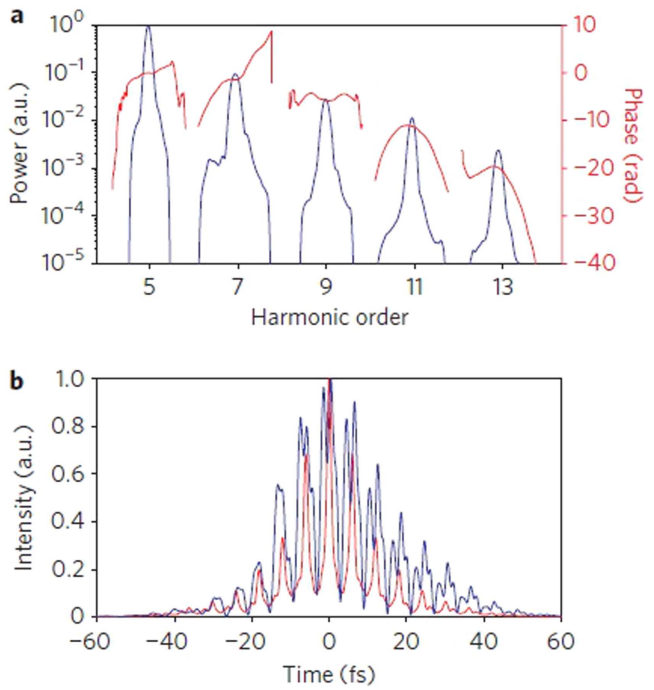

Figure 5. Reconstructed harmonics of atomic caesium, driven by a 3600 nm laser pulse at the peak intensity of 1.6 TW cm^{-2}: (a) the frequency spectrum and the corresponding phase; (b) synthesized harmonics in the time domain from the 5th to the 13th (blue) and and its Fourier transform limit (red). Reprinted by permission from Macmillan Publishers Ltd: [30], copyright 2010.

Their experimental observations and theoretical calculations both indicated that the harmonics below I_p have a clear non-perturbative negative group delay dispersion. In figure 5, we show their experimentally measured spectra and reconstructed temporal structures. As one can see, the harmonic phase decreases from the 5th harmonic to the 13th harmonic. To further examine this decreasing phase, the derivative $\partial\phi/\partial q$ was shown in figure 6 together with the calculated phase from the TDSE simulations.

In their explanation, the observed negative $\partial^2\phi/\partial q^2$ suggests a generation mechanism for BTHs similar to the semi-classical rescattering process described by the simple man's model. As we know, in the simple man's description, the short trajectories have an increasing phase with an increasing harmonic order and the long trajectories are the other way around. The observed negative group delay dispersion is an evidence supporting that these low-order harmonics are generated from the long trajectory electrons [30, 76], which is consistent with the results in [69]. They also observed a divergence angle at 15 mrad for the generated harmonics which is in agreement with the large divergence expected for the long trajectory harmonics. The above results suggest that the simple man's model is still qualitatively appropriate: the long trajectory electron wave packets can recombine with net negative energies, producing harmonics with $\hbar\Omega \leqslant I_p$ with a decreasing phase. From the results of this Keldysh-scaled system, one can infer that the NTHs from the 0.8 μm/Argon system should also have a nonperturbative mechanism.

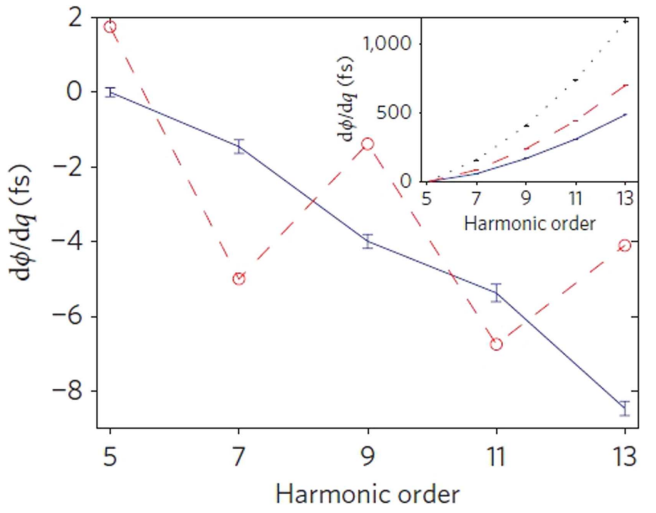

Figure 6. The harmonic phase dϕ/dq from the 5th to the 13th harmonics, extracted from the experimental data (solid) and a one-dimensional TDSE calculation (dashed trace). The inset shows the phase for a configuration of LiF window at different thickness: 2 mm (solid line), 3 mm (dashed line), and 5 mm (dotted line). Reprinted by permission from Macmillan Publishers Ltd: [30], copyright 2010.

These two experiments discussed above initialized the pursuit to reveal the underlying mechanisms of NTHs. They have shown that the simple man's model can be extended to the low-order harmonics with some modifications and approximations. After this, several theoretical works presented an improved description for this process. Subsequent experimental investigations begun to pay attention to the bound electron dynamics making use of BTHs and other properties of NTHs. We will review the experimental results in the next subsection and the relevant theoretical investigations will be reviewed in the next section.

3.3. CEP dependence and bound electron dynamics in BTHs

The applications of NTHs are not limited as a light source and the frequency comb in the VUV range, these harmonics can also reveal the bound electron dynamics. As the BTHs are generated by the electrons whose energy is less than I_p, the study of these harmonics can provide information about these bound electrons. Recently, the NTHs were investigated through a driving pulse in the DOG scheme by Chini *et al* [32]. In the DOG scheme, the driving field is composed of two circularly polarized pulses with a different rotation direction, together with their second harmonic. The overlap part of the two circularly driving pulse forms a linear window which can generate harmonics while the circularly polarized part do not affect the harmonic generation significantly. Through the control of the CEP of the linear window of this pulse, they observed a CEP dependence of BTH generation.

Their experimental results are reproduced in figure 7. In this experiment, the long trajectory contributions were not observed due to the phase-matching conditions. As we can see from figure 7(a), the observed resonance-enhanced structures are emitted in a laser-like beam since their

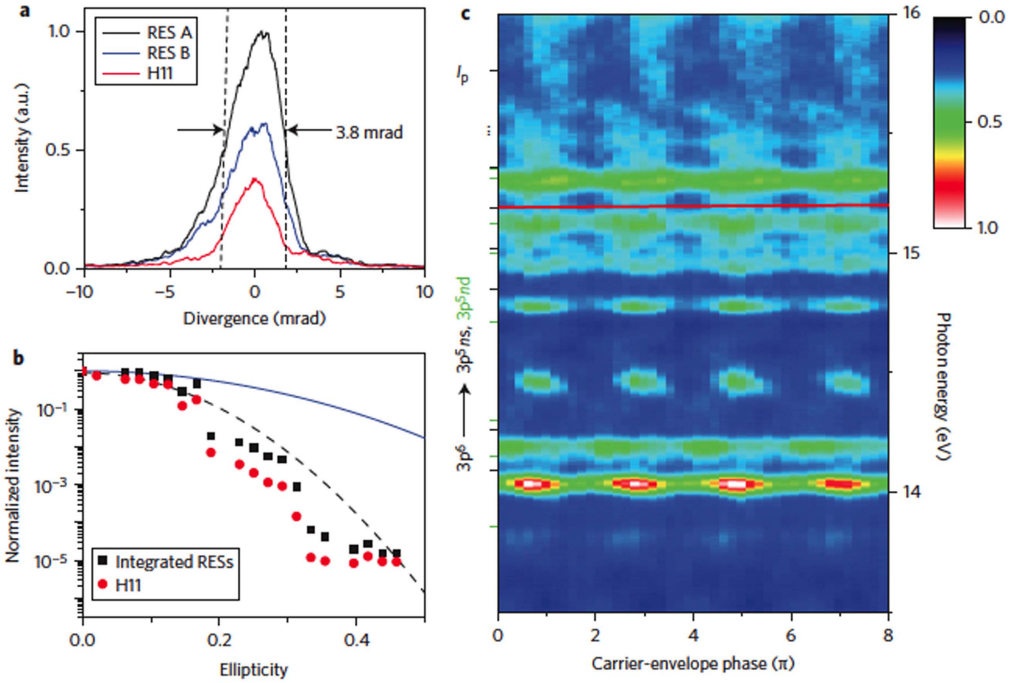

Figure 7. Field controlled features of the resonance-enhanced structures: (a) a narrow divergence angle of the resonance structures (A and B) and the above-threshold 11th harmonics. (b) The ellipticity dependence of the coherent line emission. The measured ellipticity dependence is much stronger than that predicted by the perturbative generation of the 9th harmonic (blue solid line), but agrees qualitatively with the extrapolated ellipticity dependence of the 9th harmonic from [77] (black dashed line). (c) A strong CEP dependence of resonance structures when its generation was confined to a single half-cycle of the driving laser. Reprinted by permission from Macmillan Publishers Ltd: [32], copyright 2014.

divergence angles are similar to the 11th harmonic. The observed small divergence (4 mrad) is consistent with previous measurements of BTHs in a tight focusing geometry [77]. The ellipticity dependence of the integrated yield of the resonance-enhanced structures between 15 and 15.8 eV and the above-threshold 11th harmonic is shown in figure 7(b). For both the harmonics, the observed dependence of the integrated harmonic yield on the driving laser ellipticity drops faster than predicted by the perturbative harmonic generation. The observed harmonic efficiency is reduced by an order of magnitude when the ellipticity is tuned to 0.2, while the theoretical results indicate the ellipticity should be about 0.4 when the yield drops one order of magnitude. Such a strong ellipticity dependence suggests the possibility of temporally 'gating' and manipulate BTHs by shaping the driving laser polarization.

To further explore the power of the temporally 'gating' technique for BTHs, they investigated the CEP dependence of the harmonic yield. Figure 7(c) shows the dependence of low-order harmonic generation on the CEP of the driving laser using the DOG technique, which produces an effective sub-cycle gating with the linear polarization. The observed modulation of the resonance-enhanced structure yield with a 2π periodicity is consistent with the DOG field and indicates the field control of the resonance-enhanced structure emission (usually the period is π for a short linear driving pulse). They also performed an experiment with the linearly polarized 5 fs pulses, and they found the effects of the CEP on the intensity of the resonance-enhanced structure are much weaker than that observed in the DOG field. This experiment indicated the possibility to manipulate the bound electron dynamics in an attosecond time scale through the control of the CEP of the driving field. A further theoretical investigation indicated that the CEP dependence in the low-order harmonics can also be partially explained by the semi-classical model [47].

The DOG scheme is not the only 'gating' technique to get a short linear window of the driving pulse. The direct compression of the driving pulse can restrict the harmonic in a short window as well. This kind of gating technique is called ionization gating in the generation process of attosecond pulses. Very recently, the emission of BTHs has been applied as a way to detect the dynamics of bound electrons [33] with an optical attosecond pulse. The optical attosecond pulse is compressed from a white light with a wide range of spectrum and its pulse duration is in the attosecond time scale. In the time domain, its pulse duration is less than one oscillation cycle. The pulse with the duration about one optical cycle is referred as the single cycle pulse. In the frequency domain, the optical attosecond pulse has more high frequency component (which can be understood from a Fourier transform).

In [33], the authors demonstrated that intense optical attosecond pulses synthesized in the visible and nearby spectral ranges allow a subfemtosecond control and metrology of the bound-electron dynamics. They observed the VUV spectra emanating from Krypton atoms interacting with intense waveform-controlled optical attosecond pulses. Through the analysis of the observed spectrum, they revealed

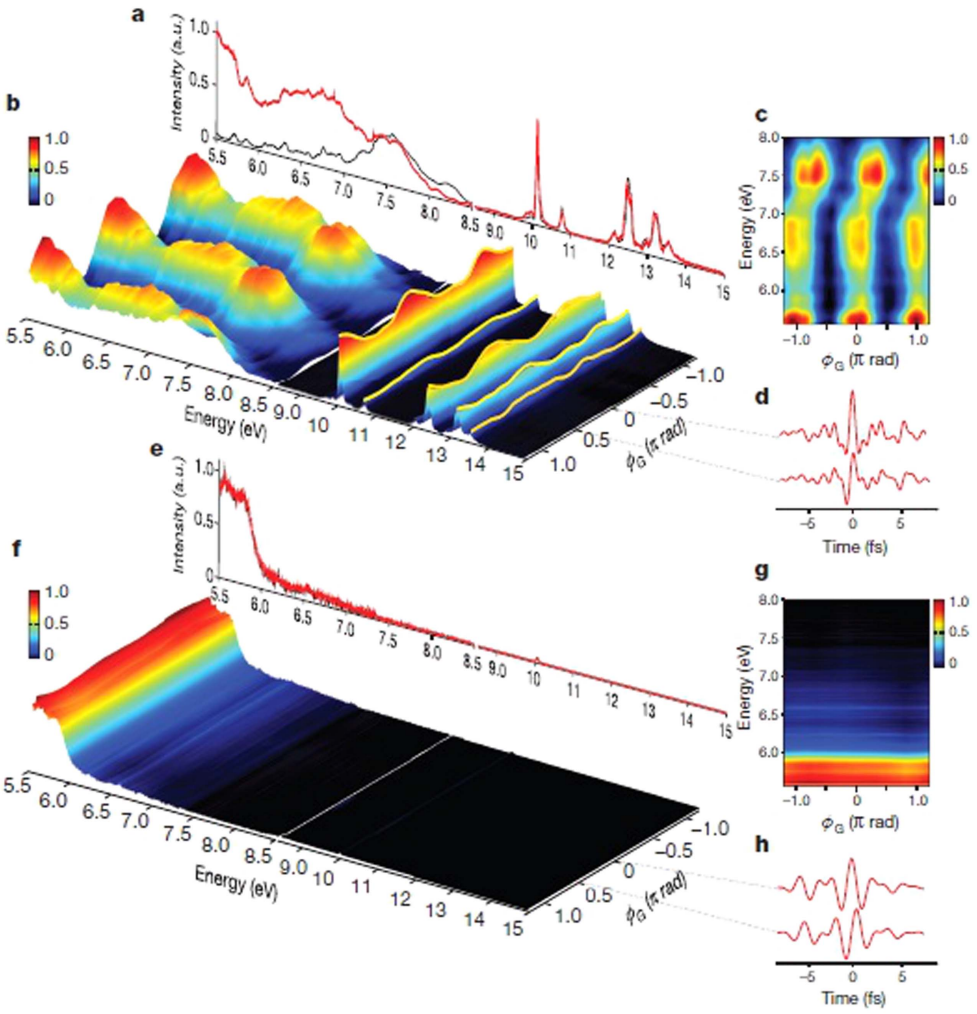

Figure 8. Attosecond control of dynamics in the bound electron of Kr. Spectrograms recorded from 5.5 to 15 eV was shown for an optical attosecond pulse in (b) and a single-cycle pulse in (f). Correspondingly, two special cases of both spectrograms for the global phase equal to 0 (red line) and $\pi/2$ (black line) were respectively shown in (a) and in (e). Part (5.5–8 eV) of the spectrograms from (b) to (f) were shown in (c) and (g). Representative driving waveforms for an optical attosecond pulse and a single-cycle pulse were respectively shown in (d) and (h). Reprinted by permission from Macmillan Publishers Ltd: [33], copyright 2016.

a finite nonlinear response time of bound electrons of up to 115 attoseconds. The experimental results also showed that the response time is sensitive to and controllable by the intensity of the driving field.

Their experimental results are shown in figure 8. Different results shown in figures 8(d) and (h) are respectively produced by different driving pulses for optical attosecond pulse (less than one optical cycle) and by a relatively long single cycle pulse (about one optical cycle). Their corresponding harmonic spectra are shown in figures 8(b) and (f) respectively. As we can see, the optical attosecond pulse can generate obvious low-order harmonics and the single cycle pulse cannot generate much signal. This may be explained as for the longer pulse, the high frequency components of the driving pulse are filtered and the low energy photons cannot excite the electron. From the harmonic spectrum in figure 8(b), one can observe the CEP dependent harmonic yield below the first excited state. The investigation of these results reveals that it takes some finite time for the bound electron to respond to the driving field. In their theoretical model, the harmonic can be written as the superposition of the 3rd and 5th harmonic. To accurately describe the experimental results, there needs to be a time delay between the 3rd and 5th harmonic, which indicates the response time of the bound electrons. This explanation were also been verified by the time–frequency analysis from the TDSE calculations.

As mentioned before, the harmonic generation process has drawn much attention because of either as light sources or as the detection tools of the atomic and molecular systems. A crucial point is how one interprets the experimental observed harmonic spectrum and extracts useful information for the detection of the interaction system. In the past investigations, different studies demonstrated how to retrieve the molecular structure, the cooper minimum, and the returning electron wavepacket from the observed spectrum. The experiment in [33] has shown us a new concept about the detection of bound electron dynamics as the application of the BTHs. However, in our opinion, the corresponding theoretical description is far

from being mature, some more deep investigations need to be carried out in the future.

3.4. Other aspects in experimental studies of low-order harmonics

The above experimental investigations revealed some physical insights into the harmonic generation near the ionization threshold. Their studies indicated the role of long trajectories in the simple man's model can also influence low-order harmonics and revealed the underlying electron dynamics during this process. The experiments have triggered more experimental studies for the harmonic generation process near the ionization potential. These further observations paid attention to other application features of these harmonics as light sources, such as the spatial distribution, the harmonic frequency range, the selection of harmonics, and the harmonic intensity for NTHs. In this subsection, we will summarize their experimental contributions in these aspects.

One of the important applications of the BTHs is as a high repetition rate coherent light source in the VUV range. The spatial distribution of the harmonic field is one of the crucial features of a light source. The spatial distribution of low-order harmonics has been investigated soon after these early experimental studies introduced above. In 2011, Hammond *et al* [34] studied the photon flux and the far-field spatial profile for the NTHs, which were produced with a femtosecond enhancement cavity-based XUV radiation source. They explored the generation of NTHs produced from Xe in a tightly focused geometry of a femtosecond enhancement cavity near 800 nm. In their experiment, short trajectories and long trajectories were observed separately. In their experiments, their observations showed that the 7th and 9th harmonic were dominated by short trajectories while the 11th and 13th harmonic were long trajectories dominated.

Along with the spatial profiles, the output frequency range is also an important issue one concerns about in any practical application. With different driving wavelengths, the wavelength of output harmonics can be manipulated. However, the requirements of the experimental conditions are different for different driving wavelengths. In 2012, low-order harmonics from a cavity are investigated with a 518 nm driving laser [35] to generate short wavelength BTHs. The driving field was generated by a frequency-doubled Yb-fiber laser with a peak intensity of 1.2×10^{13} W cm^{-2}. The interaction area was in the femtosecond enhancement cavity in the visible wavelength range. With this experimental setup, the harmonics of up to the 9th were generated with the Xe gas jet. Their investigation showed that the power of these BTHs can reach several milliwatts for the 3rd harmonic and several microwatts for the 5th harmonic. This investigation extended the wavelength range of cavity enhanced harmonics and proved the potential of the BTHs as an efficient ultraviolet frequency comb source for spectroscopic applications.

The selection of a single harmonic order is necessary in some applications such as the seeding of the free electron laser. In 2015, the selection of isolated harmonics were investigated in the BTH regime [67] through experiments. In this study, the contribution of the surrounding harmonics was totally suppressed using the interferential filtering. Within this scheme, they have analyzed and distinguished the behaviors of the generation of a single selected even order harmonic (the 6th harmonic obtained in a two-color setup) and of a single selected odd order harmonic (5th harmonic in a single-color setup). In their investigations, they found that the fundamental laser beam aberrations can cause the appearance of a non-homogenous donut-shape in the spatial profile of the 6th harmonic. However, this undesirable effects can be easily controlled, indicating that the spatial quality of a selected even harmonic can be as good as that in the usual odd harmonic generation.

Apart from the above studies in various features of low-order harmonics, the enhancement of the yield of high-order harmonics has also been attempted experimentally, making use of BTHs. In 2013, Brizuela *et al* [68] investigated a scheme using the BTHs as a seed source to enhance the yield in the HHG process. They introduced a scheme based on using BTHs, generated in a 'seeding cell', to enhance the HHG process in a 'generation cell', placed along the direction of the driving field. By modifying the fundamental driving field, the ionization step of the nonlinear HHG generation process in the 'generation cell' can be manipulated by the low-order harmonics generated in the 'seeding cell'. The purpose of this dual-cell scheme was to enhance the conversion efficiency of HHG so that one can have a realization of robust intense attosecond XUV sources. Their simulations showed that the enhancement factor can be scaled far above one order of magnitude by increasing the low-order harmonic intensity. As the increase of yield of HHGs is a experimentally challenging problem, the experimental scheme here brought us a clue to solve this kind of problems in applications using nonlinearity of the HHG sources.

All these experimental work reviewed above have provided us with a lot of knowledge about NTHs from the basic underlying physics to crucial properties as a light source. We have gained much intuitive understandings about the harmonic generation in this regime. As we mentioned, the theoretical description of NTHs is quite complicated, due to the important impact by the Coulomb potential and the resonance effects of many bound states. There have been many great advances in the theoretical understanding, we will cover these comprehensive theoretical investigations in the next section.

4. Theoretical investigations of NTH generation

Aroused by the recent experimental studies, there have been many theoretical works using different kinds of methods. In this section, we will review recent theoretical investigations on NTH generation.

We will start from investigations with the perturbation theory [44], which is applicable to describe the low-order harmonics when the laser intensity is relatively weak. Then we will review the theoretical progress which has been gained by the TDSE calculations [45, 78]. The numerical solution to

the TDSE is an accurate method for the description of NTHs within the SAE approximation. By scanning and tuning many parameters of the laser pulses, one can extract features of NTHs from the TDSE calculations to identify the underlying mechanisms such as the quantum path interferences and the resonance effects.

As mentioned before, the concept of the quantum path comes from the SFA. Investigations have verified that the basic picture from this model can still help us understand some features in the low-order harmonic generation process, although the accuracy of the SFA is not guaranteed in this region due to the strong impact of the Coulomb potential. In addition, the semiclassical description of low-order harmonics [46, 47, 79] has been well developed recently and has helped us to intuitively clarify the underlying mechanisms for many important phenomena in BTHs. Along with the time–frequency analysis [48, 49], the classical methods can provide a clear picture of this process. At the end of this section, we will review recent theoretical investigations about the BTH generation in molecules [80–84]. As we can see, for molecules, there are more degrees of freedom to be manipulated in the process of BTHs.

When it comes to BTHs, the generation of attosecond pulses from these harmonics is an interesting topic. Henkel *et al* [85] investigated the VUV generation from a model neon atom driven by a linearly polarized pulse and a polarization gating pulse. They compared HHG in the linearly polarized laser pulses to the method of polarization gating. They found that attosecond pulses can be generated at the Fourier limit of 700 as given by an indium filter, spectrally centered at 15 eV. Their investigation verified the possibility to use the polarization gating technique to generate attosecond pulses in the low-order harmonics.

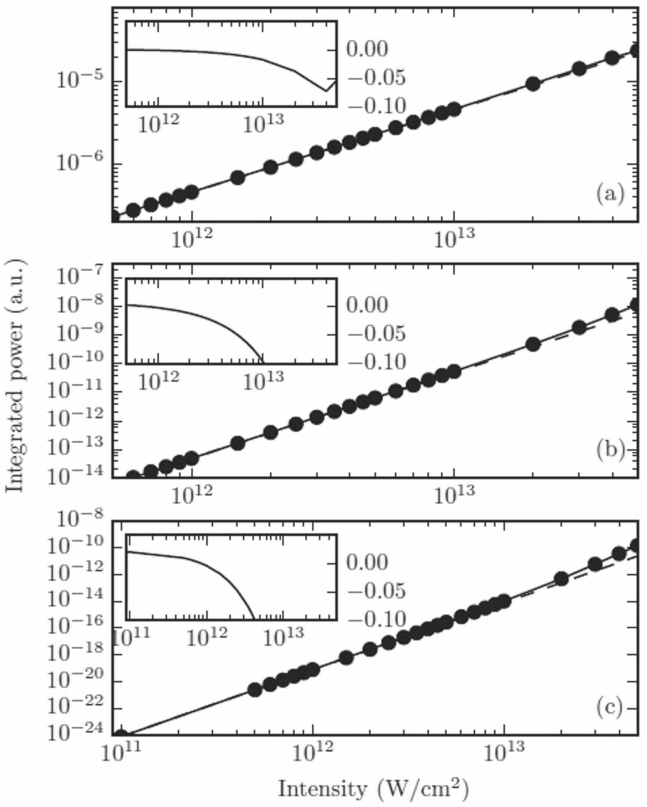

Figure 9. Comparisons of the integrated harmonic yields as a function of the peak laser intensity, for (a) 1st, (b) 3rd, (c) 5th order, between the *ab initio* calculations (solid circles with solid lines) and a perturbative I^n power-law fit which was matched to the *ab initio* results at the lowest intensity. The insets shows the relative error between the two results. In all the calculations, a 1600 nm laser pulse with 10 optical cycles was adopted. Reprinted figure with permission from [44]. Copyright 2015 by the American Physical Society.

4.1. Breakdown of the perturbation theory

The perturbation theory was thought to be useful in explaining the experimental observation of the low-order harmonics. Recently, the transition from the perturbative regime to the non-perturbative regime for NTHs is investigated in [44].

They presented the results of accurate numerical calculations and perturbative calculations for the low-order harmonics. By comparing the *ab initio* calculations and the perturbative results, they found that the transition from the perturbative to the nonperturbative interaction occurs around the laser intensity of 10^{13} W cm^{-2} at the laser wavelength of 1600 nm. These findings confirmed previous results that the perturbative treatment needs to be replaced by a non-perturbative treatment for the BTHs.

The integrated harmonic yield of 1st, 3rd and 5th harmonic from the TDSE calculations and the perturbative power law are shown in figure 9. In their investigations, the driving laser intensity was increased from 10^{11} to 10^{14} W cm^{-2} at a wavelength of 1600 nm with a pulse duration of 10 cycles. The power law says that for the nth harmonic, the harmonic yield satisfies $M(\Omega) \propto I_0^n$. The insets show the relative error between the *ab initio* results and the power-law predictions. As we can see, the higher the harmonic order, the sooner it does not satisfy the power law. For the first harmonic, the power law become inaccurate when laser intensity is larger than 10^{13} W cm^{-2} while for the 5th harmonic, this critical value is reduced to around 10^{12} W cm^{-2}. Their results showed that, for these laser parameters, the harmonic generation process gradually becomes non-perturbative for low-order harmonics.

As expected, the perturbation theory cannot provide accurate results for strong laser fields, which means that the higher order perturbation is larger than the lower order perturbation when the driving laser intensity is strong. Nevertheless, the concept of multiphoton process can still be generalized to the case of an intense field. For example, in a usual harmonic spectrum one can observe separated odd harmonics. To explain these harmonics, one can attribute this phenomenon to the interference of electrons ionized at different half cycles, or one can interpret the phenomenon as a N-photon transition, considering the symmetry of the atomic system. This concept of the multiphoton transition is quite useful in the low-order harmonic generation for resonance effects or the bound electron response time [33], which will be discussed later in this section.

4.2. Quantum path interferences and resonance effects studied by TDSE

As one knows, the accurate theoretical method on the harmonic generation is based on the numerical solution to the TDSE. For instance, in the recent study on the interference structure in the yield of BTHs [29], the comparisons between the TDSE results and the experimental data are very good. One of the advantages of the TDSE calculations is that, as long as the stability and the convergence of the numerical method is guaranteed, it can be applied to extract the harmonic spectrum in any energy range at different laser parameters. In this way, one can identify many mechanisms underlying the phenomena in NTHs with a large amount of calculated spectra.

In this subsection, we are going to review several theoretical studies based on the TDSE calculations. In particular, we will focus on the quantum path interference and the resonance effects in BTHs.

4.2.1. Quantum path interferences. In the experiment in 2008 [29], the intensity dependent quantum path interference [59] was investigated and the phases of different trajectories were calculated. As described before in equation (10), the harmonic yield can be affected by the phase difference of S_1 and S_2. This phase is considered to be the phase that the electron accumulates during its propagation in the driving field and it can thus be influenced by both the peak intensity and the wavelength of the driving laser.

The wavelength dependence of harmonic yield has been extensively investigated when a mid-infrared pulse is applied to extend the cutoff energy ($3.17U_p$) of high-order harmonics [56, 86–98]. These investigations indicated that when the wavelength λ increases, the harmonic yield decreases as $\propto\lambda^{-5}$. Besides, the quantum path interference structure can also be observed [88, 90] when one scans the harmonic yield as a function of λ in a very small spacing. In experiments, the driving laser intensity is easier to control continuously and the interference structure looks like steps as the harmonic yield increases rapidly with the increase of the laser intensity [29]. However, the fast increase of the harmonic yield and the saturation effect forbids one to investigate this phenomenon in a larger parameter range.

Comparably speaking, the interference structure can be easier to be observed when one changes the wavelength, as demonstrated in a recent study [45]. In this study, the harmonic yields with different driving wavelengths were calculated by the TDSE calculations for a 20-cycle pulse at a peak intensity $I_0 = 6 \times 10^{12}$ W cm^{-2}. The wavelengths varied from 702 to 1080 nm with a small space $\delta\lambda = 1$ nm. Their results are shown in figure 10. As seen from this figure, the spectra from the 5th to the 11th order oscillates with the change of the wavelength and show complicated structures. By detailed studies, they found that these structures are contributed both by the quantum path interference and by the resonance effect, which will be discussed below. In figure 10, besides these structures changing with the wavelength, there exist photon emissions at almost fixed photon energies for all

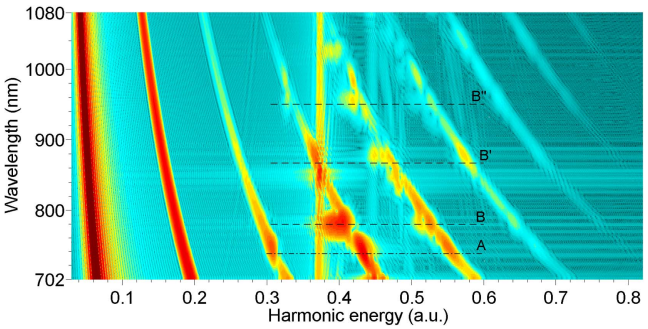

Figure 10. The low-order harmonic harmonics of hydrogen atom, driven by an intense laser pulse at a peak intensity of $I_0 = 6 \times 10^{12}$ W cm^{-2} at various wavelengths from 702 to 1080 nm. Reprinted figure with permission from [45]. Copyright 2014 by the American Physical Society.

wavelengths, among which one of the most significant ones is at photon energy of 0.375 a.u.(corresponding to the transition from the 2p to 1s state). These emissions are similar to resonance structures recently observed in the DOG scheme experiments [32]. Please note that, these emissions normally can be understood when the resonance happens for a certain photon energy. However, the authors showed that [45], for the wavelengths whose photon energies do not satisfy the resonance condition, the excitation mechanism can be a quasi-static excitation since it is insensitive to the wavelength and the laser ellipticity. The ellipticity insensitiveness of these emissions, may be related to the observed abnormal ellipticity dependence for a certain order of harmonics discussed earlier [23–25].

In order to disentangle the two mechanisms contributing the complicated structures in figure 10, the authors calculated the integrated yields of the 5th, 7th, and 9th harmonic as a function of the wavelength (from 702 to 820 nm) at various laser intensities, as shown in figure 11. Immediately, one can see that all the three harmonic orders have two series of peaks marked as 'A' and 'B' respectively. It turns out that the peak 'B' is mainly caused by the quantum path interference while the peak 'A' is mainly contributed by the resonance effects.

Here, we first look at the quantum path interference and the resonance effects will be discussed later. In the investigation on the dependence of the harmonic yield on the wavelength, interference structures have the same physical origin with that of the intensity dependent interference structures. Both of them can be explained by the quantum path interference in the SFA as discussed before with equation (10). In the description of SFA, one can go one step further about the interference structures. It can be deduced that the quantum path interference is related to the channel closing number defined by $R = \frac{U_p + I_p}{\omega}$ [88, 99]. Gentle interference peaks will emerge while R is a little smaller than an integer if the ground state of the Coulomb potential is used in the calculations. The harmonic yields in BTHs cannot be accurately estimated by the SFA, while the concept of quantum orbits can be generalized to understand this phenomenon. For the case of BTHs, the contributing

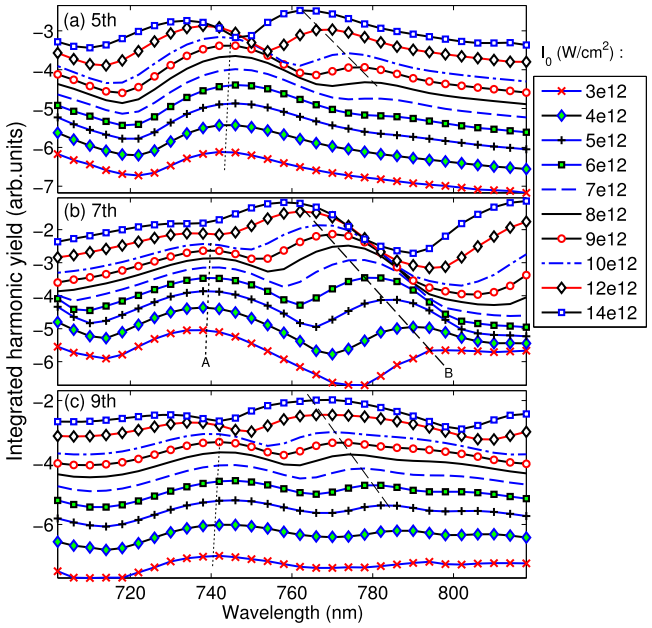

Figure 11. Two sets of resonance structures appear in the integrated harmonic yield as a function of the wavelength at various peak intensities, for: (a) 5th, (b) 7th, and (c) 9th harmonic. Reprinted figure with permission from [45]. Copyright 2014 by the American Physical Society.

electrons with the long quantum orbits will return to the core after its excursion in the laser field for about one optical cycle. From a simplified quantum path interference model, the superposition of these long orbits and the short orbits with a near zero phase can also lead to interference peaks spaced by $\delta R \approx 1$. These interference peaks can be observed in the harmonic spectrum. In their results shown in figure 11, the position of peak 'B' at all laser intensities satisfy $R \approx 8.8$. These observations suggest that these peaks are mainly contributed by the interferences of generalized short and long quantum orbits in the BTH region.

4.2.2. Resonance effects. We now come to discuss the series of structures maked by peak 'A', which are mainly contributed by the resonance effects. Actually, the resonance effects had been investigated for the HHG soon after the method of the numerical solution to the TDSE was developed. In the resonance phenomenon, the harmonic yield can be enhanced due to the existence of bound states. The bound states act as an intermediate state when the electron gets ionized or before its recombination. In 2000, through the TDSE calculations, Gaarde *et al* [100] investigated the resonant multiphoton population transfer in potassium atoms. They found that the amount of electron population transferred to the excited state as a function of wavelength and intensity shows clear signatures of resonances. This phenomenon was further investigated by using a chirped laser pulse to temporally resolve the process. They concluded that the resonant process competes strongly with the direct, nonresonant ionization of the ground state. Later in 2001 [101], they continued to investigate the enhancement of many high-order harmonics via a single multiphoton resonance. They calculated the harmonics generated subjected to a long mid-infrared radiation. They found that several harmonic orders are enhanced through a single multiphoton resonance over a wide range of intensities, and that the width of the enhanced harmonics is governed by the lifetime of the multiphoton resonance states. This investigation revealed that it is possible to enhance neighboring harmonic orders via a single resonance if the multiphoton transition matches the energy difference between the ground state and an excited state. After that, Maquet's group performed systematical study of the roles of resonances and recollisions in both the above threshold ionization [102] and the high harmonic generation [103].

In principle, the low-order harmonics are more easily to be affected by the bound states of the atomic potential since the photon energies involved are close to the energies of the excited states [45] performed some detailed studies to the resonance effects in BTHs. The authors found that the resonances can happen both in the ionization step and the recombination step. This means that the bound states can act as intermediate states either in the ionization step or the recombination step. The resonance in the ionization step happens when $\Omega = n\omega$ matches the energy gap between the ground state and a certain excited state. In this case, the electron is easier to get excited to and ionized from the excited state. This can be observed from the fact that the harmonic yield can be enhanced for some certain wavelengths. Peak 'A' shown in figure 11 is just one of them, which can be identified as a 6-photon resonance with the shifted $|n = 2\rangle$ state. This is similar to the previous investigations that several harmonics can be enhanced through a single resonance. For a resonance in the recombination step, it means that for the electrons with the long trajectories, they can be trapped in Rydberg states before their recombination. The trapping of these electrons may influence the phase accumulated in the propagation step and may smear out the interference structures for a certain harmonic energy ($\hbar\Omega \approx I_p$).

After this, some further investigations have been performed for the resonance enhancement in He atom by Camp and coworkers [78]. In their studies, the wavelength of the driving field in the TDSE calculations varies from 425 to 500 nm and the intensity changes from 3×10^{13} to 1.4×10^{14} W cm^{-2}. They identified that through the multiphoton resonances between the ground state and the Stark-shifted 1s2p, 1s3p, and 1s4p excited states, 7th, 9th, and 11th harmonic are enhanced. Their numerical results for the integrated 9th harmonic are shown in figure 12. For the 9th harmonic, an Autler–Townes-like splitting of the enhancement feature due to the 3p state can be clearly observed. The splitting of this enhancement happens when the wavelength and intensity of the driving field strongly couples the 3p state to the nearby dark 2s state. They also performed a time–frequency analysis of these emissions and the results showed that both the short and the long quantum path are enhanced through these resonances.

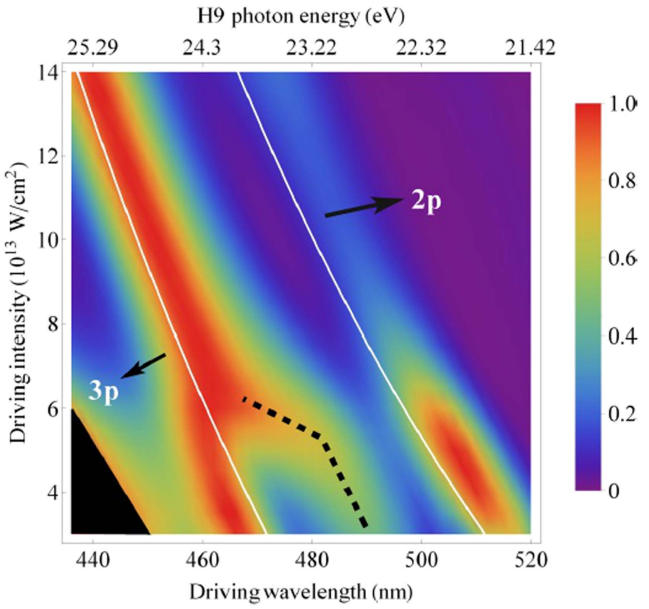

Figure 12. The integrated yield of the 9th harmonic as a function of both the wavelength and the peak intensity of the driving laser. The white lines mark the photon energies of resonant enhancements due to the 2p and 3p states, while the dashed black line highlights the Autler–Townes splitting of the 3p state. Reprinted figure with permission from [78]. Copyright 2015 by the American Physical Society.

4.3. Various progresses made by semiclassical methods

We mentioned that the concepts of trajectories are still useful in describing the harmonic generation near the ionization threshold. Actually, recent studies showed that semiclassical methods such as CTMC simulations can help us to understand many interesting phenomena in low-order harmonics.

For the explanation of interference structures identified in the experiment of [29], the authors already suggested the contribution of the long trajectories to the BTHs. After that, Hostetter *et al* [46] performed a classical simulation for the electron trajectories to visualize these quantum paths. In their model, they assumed the electron travels under the interaction of both the laser field and the Coulomb potential. The electron energy is calculated by the summation of the kinetic energy and the potential energy. When the electron returns to the core, it is possible for the electron to have a negative energy, which corresponds to the emission of a photon energy less than I_p if the electron recombines to the core. A typical evolution of the electron trajectory and its energy as a function of time are shown in figure 13. As one can see, these electrons are ionized at the peak of the driving field. When they return to the core, the kinetic energy is rather small and the total energy is negative due to the negative potential energy. They found that these electrons can contribute to the BTHs and their phase information agrees with the calculations in [29] and the performance of these long trajectories are not sensitive to the choice of initial conditions of the electrons.

After this classical model, the semiclassical description for BTHs has been developed in two directions. On the one hand, a more accurate semiclassical model (CTMC) has been developed to calculate the final harmonic spectrum. On the other hand, those classical trajectories have been compared with the time–frequency results from the TDSE calculations to reveal more reliable electron dynamics. Here we will summarize these studies which have extended the semiclassical model in the BTH regime.

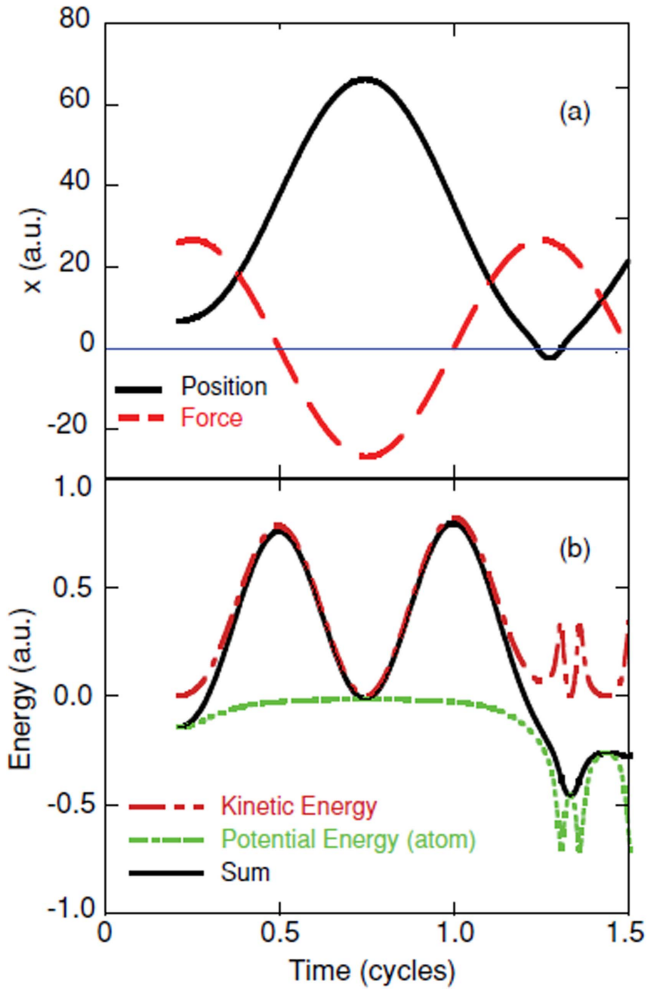

Figure 13. Trajectory-based analysis in the generalized semiclassical model by including the Coulomb potential. (a) the position of the electron as a function of time. The dashed (red) line represents the force from the laser field. (b) the electron energies for the same trajectory shown in (a). The laser intensity is 10^{14} W cm^{-2} and the return energy is about −0.25 a.u. Reprinted figure with permission from [46]. Copyright 2010 by the American Physical Society.

4.3.1. Half-cycle cutoffs in below threshold harmonic generation. The CTMC method has been introduced in section 2. The advantage of this method lies in the description of trajectories of low-energy electrons with the Coulomb potential taken into consideration. The CEP dependence of high-order harmonics is related to the ionization rate and the classical trajectory. The CEP dependence in the high energy part has been successfully explained within the classical model [104, 105]. When it comes to BTHs, the CEP dependence effect has also been experimentally observed in a DOG setup [32]. Recently, Xiong and coworkers [47] have

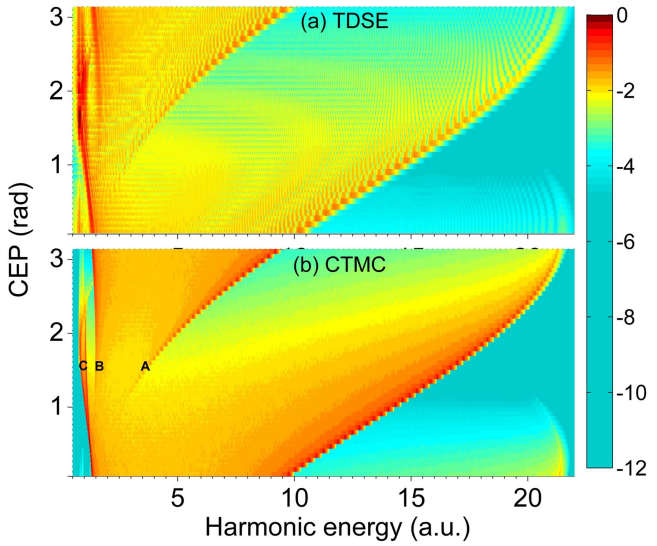

Figure 14. The harmonic spectra (in the log scale) from a SAE helium driven by an intense mid-infrared pulse, calculated by TDSE in (a) and by CTMC in (b) respectively, at various CEP ϕ. For the case of $\phi = \pi/2$, A, B, marks the low energy cutoffs and C marks the high energy cutoff. Reprinted from [47] under a Creative Commons Attribution 3.0 Unported (CC-BY) license.

used the CTMC method to explain the CEP dependence in the low-order harmonics. In the tunneling regime, they found that the CEP dependence of low-energy harmonics can be well explained through a CTMC model. The agreement between TDSE and CTMC model is rather good even for the low-order harmonics.

In figure 14, their harmonic spectra [47] are shown for a model He with the model potential

$$V(r) = -[1 + (1 + 27r/16)\exp(-27r/8)]/r. \qquad (16)$$

The driving field is at 1800 nm with a peak intensity of 7×10^{14} W cm^{-2} and has a pulse duration of 2.3-cycle full width in a sin-square pulse shape. Please note that, the choices of the laser parameters and the atomic helium ensures the ionization happen in the deep tunneling region so that the ionization probabilities can be correctly assigned in the classical simulation. In addition, the selection of He atom with a large ionization potential can effectively avoid the significant bound–bound transition [45]. These are crucial to make the CTMC method applicable so that one can discuss the classical trajectory effects on the BTHs.

As can be seen from figure 14, the whole spectrum calculated by the CTMC method agrees well with that from the TDSE. If one looks at the high energy part, the well understood high-energy half-cycle cutoffs can be clearly observed in both methods. At the energy range around the ionization potential about 0.9 a.u., some CEP-dependent structures can also be seen in both figures 14(a) and (b). From these two figures, one can observe that with the decreasing harmonic energy, the harmonic yield has a sudden drop near the ionization potential, this sudden drop can be identified as a low-energy cutoff structure. when the CEP ϕ increases from 0 to about 1.6 rad, the position of this low energy cutoff moves toward a lower energy. When ϕ is further increased, the spectrum becomes complicated due to the multiple return trajectories. This investigation showed that the low energy cutoff have the same classical origin as the high energy cutoff. The returning electrons have a minimum recombination energy for short driving pulses and this minimum energy is dependent on the CEP.

Through a careful study of the low-energy cutoff, this investigation further identified the roles of the multiple-return trajectories and the effects of the ionic potential. Although the impacts of these two were usually difficult to be directly observed in the harmonic spectrum, both of them can be explicitly demonstrated with the reference of the low-energy cutoff structure. In addition, they found that the CEP dependence of BTHs is very sensitive to the driving pulse duration. This observation was in agreement with the DOG setup [32] experiment where the CEP dependence of the harmonic yield disappears for a 5.5 fs linear driving pulse.

4.3.2. Correspondence between NTHs and the frustrated tunneling ionization. Along with the ionization process and harmonic generation process, the creation of Rydberg states is another important phenomena when atoms or molecules are subjected to an intense laser field. The latter has been dubbed the name of frustrated ionization in 2008 [106]. Later on, Landsman and coworkers [107] carried out a detailed study about the similarities and differences between the HHG and the creation of the Rydberg atoms through the laser ellipticity dependence. They found that the two processes involve electrons tunneling at different time: the HHG electrons tunnel out after the peak of the electric field and then recombine with the core, while the *dominant* FTI electrons tunnel before the peak and do not come back to the core. In addition, it has been showed by Liu *et al* [108] that FTI is related to the partial atomic stabilization observed in strong infrared fields. From a detailed semiclassical analysis, they found that there are actually two different types of orbits contributing to the creation of Rydberg atoms: directly launched into the elliptical orbits (type 1) or ejected after collisions with the core (type 2).

In a recent theoretical work, Xiong *et al* [79] bridged the two processes of the BTH generation and the creation of low-lying Rydberg atoms (mainly via type 2 orbits) through the frustrated tunneling ionization. In this work, an underlying correspondence relationship is identified between these two processes with the CTMC and TDSE calculations. The yield of BTHs and the population of low-lying Rydberg atoms can be simultaneously manipulated by the control of the CEP of the laser pulse. The electrons that generate the BTHs and the Rydberg atoms are both low energy electrons, they are both ionized around the peak of the driving field. In the theoretical calculations, these two phenomenon have a similar CEP dependence. Some further semiclassical investigations showed that they share a similar bunch of electron trajectories.

In figure 15, the yields of BTHs (left column) and the population of Rydberg states (right column) are shown as a function of the electron energy at different CEPs of the pulse

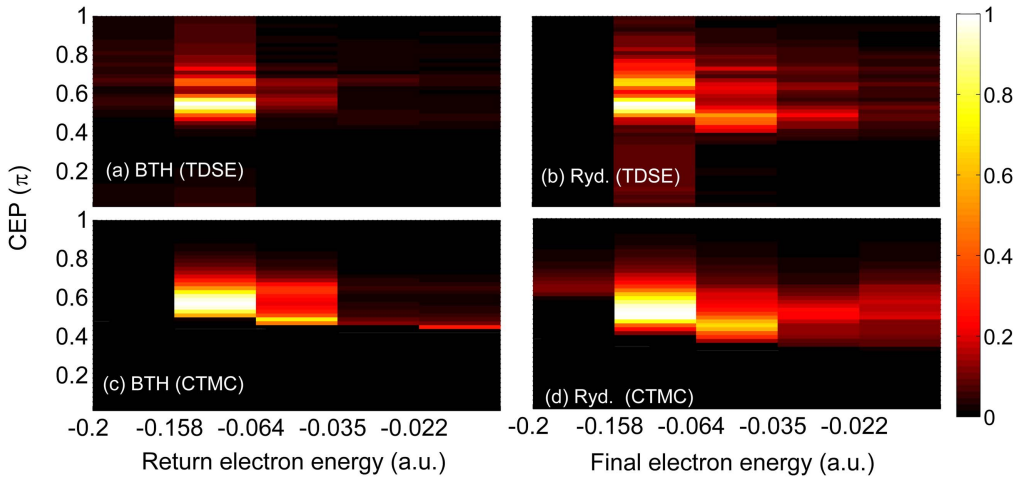

Figure 15. The BTH spectra and the low-lying Rydberg state population as a function of the return electron energy. Comparisons are made between the results by TDSE in (a), (b) and by CTMC in (c) and (d), for different CEP ϕ of a 2.3-cycle $\sin^2$ pulse with a wavelength of 1800 nm and a peak intensity of 7×10^{14} W cm^{-2}. Reprinted figure with permission from [79]. Copyright 2016 by the American Physical Society.

calculated by the TDSE and the CTMC respectively in the work of [79]. The laser parameters are the same as those in the figure 14. Each harmonic energy was subtracted by the value of the ionization potential I_p, which makes the horizontal axis of figures 15(a) and (c) the return electron energy at its recombination instead of the photon energy. Besides, as the Rydberg states calculated by TDSE in figure 15(b) are represented by blocks in the energy axis because bound-state energies are discrete. For example, the energy of the $|n = 2\rangle$ state is -0.158 a.u. and the energy of the $|n = 3\rangle$ state is -0.064 a.u. These energy differences are chosen to be the center of the energy blocks we use here in this figure. The same energy block was used for the harmonic spectrum in other figures of figure 15 for a better comparison. As one can see, the results from the CTMC simulations (lower) agree quite well with those of the TDSE calculations (upper). The striking features are that the CEP-dependence of BTHs and Rydberg population is very similar, both dominated in $\phi \in (0.5\pi, 0.7\pi)$. Some further investigations revealed that the electrons which generate the BTHs and which are trapped in Rydberg states share similar initial conditions. When the CEP changes, these electron trajectories change in a similar way, which leads to the similar CEP dependence of the BTHs and the Rydberg state populations. This investigation indicates the classical description is qualitatively correct for both the low-energy harmonics and the Rydberg atom creation when the lower excited states are not closely coupled with the ground state via multiphoton resonances.

4.4. Time–frequency analysis for NTHs

As mentioned above, the classical trajectories have been compared with the time–frequency results from the TDSE calculations in the BTH regime. The time–frequency analysis is a well developed tool in the numerical solution to the TDSE to extract the emission time of in high-order harmonics [53–55]. The recombination time from semiclassical models can have rather good agreement when compared with the time–frequency analysis from the direct solution to the TDSE. For low-order harmonics, due to the small photon energy, the time resolution of the time–frequency analysis is rather limited. However, recent studies [48] showed that the time–frequency analysis through a synchrosqueezed transform (SST) can have some agreement with the classical trajectories and the agreement provides the dynamics of these low energy electrons. Previously, we have mentioned the application of time-frequency to the role of resonance and the electron response to the driving field. Here we will review some results using time–frequency analysis to identify the classical trajectories for low-order harmonics.

In 2014, Li *et al* [48] presented an *ab initio* investigation on the BTH generation of He atoms in few-cycle infrared laser fields by accurately solving the TDSE and Maxwell's equation simultaneously. They found that the enhancement of the BTH generation only occurs to near the resonance structure of He. With the help of the quantum and semiclassical trajectories analysis, as well as the SST of the harmonic signal, they revealed that the contribution of several multirescattering trajectories to the resonance-enhanced BTH generation. Figure 16(a) shows the time–frequency analysis of the harmonic spectra of He by the Gabor transform, along with the corresponding semiclassical result. However, from figure 16(a) it is difficult to recognize the contributions of the individual rescattering and multirescattering trajectories in the near- and below-threshold regions due to the limitation of the time resolution of the Gabor transform and several time–frequency profiles with different ionization peaks are superposed. Figure 16(b) shows the SST time–frequency analysis of the same spectra. As one can see, the results from SST are clearer than that from the Gabor transform. By comparing with the classical calculations, the multirescattering trajectories, mentioned before [47], can be clearly seen in the figure. These trajectories are marked by the yellow arrow and have strong contributions to the NTH and BTH whose

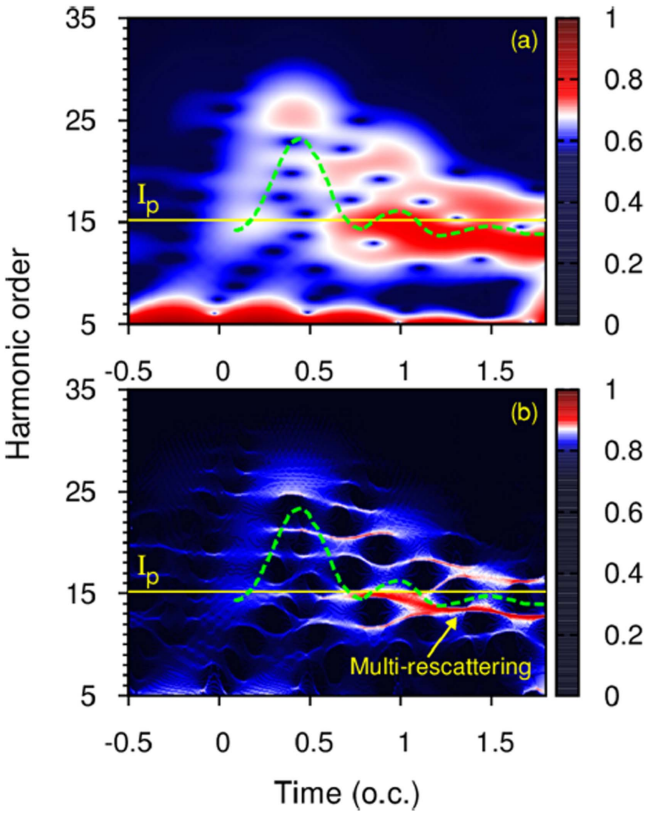

Figure 16. (a) The analysis of the harmonic spectra of He by the usual Gabor transform. (b) the time–frequency analysis by the SST for the same spectra. The laser intensity is 9×10^{13} W cm^{-2} and the wavelength is 760 nm. The green dashed line indicates the corresponding semiclassical result and the yellow solid line indicates the ionization potential I_p. Reprinted figure with permission from [48]. Copyright 2014 by the American Physical Society.

corresponding harmonic orders are from 13th to 15th. The good agreement between semiclassical result and SST result means that the SST is capable of revealing the characteristic behaviors of harmonic spectra below the ionization threshold. In the time–frequency or the semiclassical model, the concept of multirescattering trajectories can be defined and their contribution can be observed. However, in a realistic experimental measurement, we do not have the time resolution as the time frequency analysis to observe the contribution of harmonics emitted at different times. Thus, the multirescattering trajectories cannot be directly observed in the harmonic spectrum. But as recently discussed [47], the effects of these multirescattering trajectories in the harmonic spectrum may be observed with the help of low-energy cutoff structure for a very short laser pulse.

The above investigations demonstrated that one can already observe the dynamics of the low energy electron with the help of time–frequency analysis and the classical model. In 2015, a further study [49] investigated electron dynamics from the NTH and BTH generation of Cs with the SST method and classical model. They performed a TDSE calculation of the NTH and BTH generation of Cs atoms in an intense 3600 nm mid-infrared laser field. Combining the SST spectrum and a semiclassical analysis, they were able to clarify the electron dynamics during this harmonic generation process.

We reproduce their main results in figure 17. The time–frequency representation in figure 17(a) shows the recombination time of short and long trajectories. As we can see in the time–frequency calculations, the main contribution to the high-order harmonics is due to the short trajectories. Figure 17(b) is a enlarged view of the low order harmonics. In this figure, the trajectories between the 9th and 13th harmonic suggest the contribution of multiple return trajectories, and the prominent trajectory located near the vicinity of the 7th harmonic may be caused by the resonance effects.

The semiclassical results are presented in figures 17(c) and (d). The short trajectories 1, long trajectories 2 and the multiple return trajectories 3 (second return) from the classical model can be clearly observed for high-order harmonics. For BTHs, the trajectories that released late and return early are regarded as the below-threshold short trajectories 4, and those released early and return late are labeled as the below-threshold long trajectories 5. The trajectories marked by 6 are the resonant trajectories. These trajectories are released and almost immediately return. They can only contribute to the near resonance 7th harmonic.

The combination of the time–frequency analysis and the classical trajectories further verified the classical description for the BTHs. Although the accurate calculation of these harmonics through a semiclassical model is difficult at the present, the basic concepts has been widely accepted.

4.5. NTHs in molecules

The investigations for low-order harmonic generation process have recently been extended to molecules. As the molecules have more complex structure and more degrees of freedom, many additional interesting phenomena can be observed. For example, the abnormal ellipticity dependence in molecules is also influenced by the alignment angle of the molecular axis with respect to the laser polarization. Besides, the studied phenomena in molecular HHG can also be observed in NTHs, such as the ellipticity of the harmonic emission, the odd harmonics, the interference structures, and so on. In this subsection, we will first review the abnormal ellipticity dependence in molecules and then summarize the extension of some molecular HHG phenomena to NTHs.

Different from atoms, molecules have multiple centers and their alignment angle can be manipulated. As has been discussed in [30], the ellipticity dependence of harmonic yield in molecules is influenced by the alignment angle. After the experimental observation in [30], a theoretical work based on the time dependent density function theory (TDDFT) [80] also found a similar abnormal harmonic spectrum in molecules. But the physical mechanism of these abnormal ellipticity dependence is still not fully understood yet. They investigated the ellipticity dependence of the NTHs of aligned H_2 molecules using TDDFT. The abnormal ellipticity dependence of the harmonic yield was observed in the calculated results. They suggested the anomalous maximum for

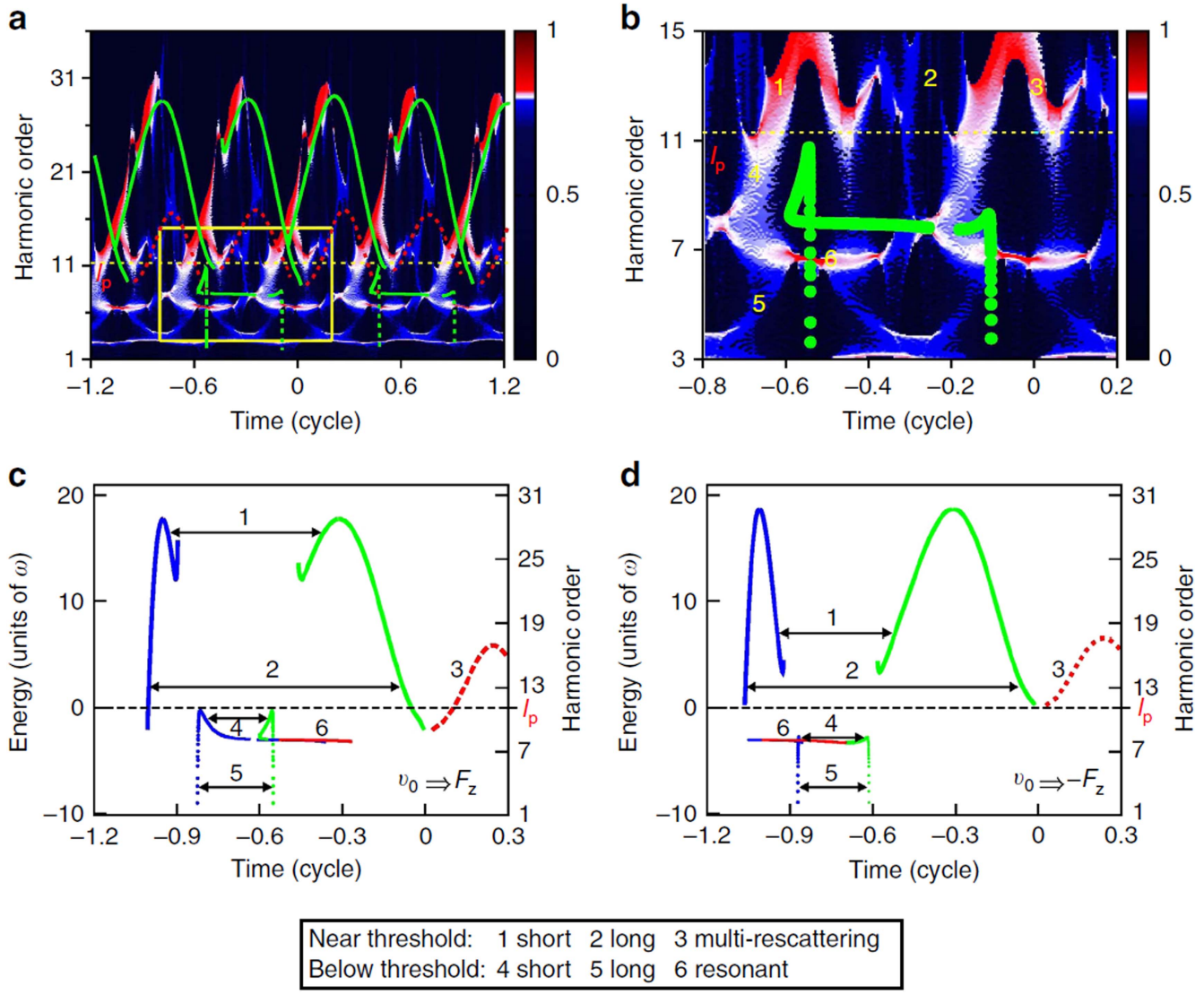

Figure 17. (a) A time–frequency analysis by the SST to the HHG spectra from Cs atom driven by an intense mid-infrared at the intensity of 1.4×10^{12} W cm^{-2} and wavelength of 3600 nm. The green curves (both solid lines and dots) and the red dashed lines indicate the semiclassical trajectories of the first return and second return, respectively. (b) An enlarged view of the SST time–frequency profiles in the near- and below-threshold regions (marked by the yellow window in (a)). (c) Semiclassical return energy as a function of ionization time (blue lines) and return time (green lines and red dashed lines). (d) Same as (c), except that the electron's initial velocity is released against the electronic-field force. Reprinted from [49] under a Creative Commons CC-BY license.

the NTHs in H_2 can be attributed to multiphoton effects of the orthogonally polarized component of the elliptically polarized laser field. Their calculations also showed that the structure of the molecules, such as molecular orientations and bond length, can be reflected on the ellipticity dependence of the NTHs.

In figure 18, we show their calculated spectrum of the generated harmonics for H_2 molecules. Each harmonic is normalized to the harmonic intensity at $\epsilon = 0$. The anomalous maxima can be clearly observed in the NTHs. For the perpendicular alignment (figure 18(a)), the 5th as well as the 7th harmonic reaches its maximum intensity at $\epsilon \approx 0.2$. For the parallel alignment (figure 18(b)), an anomalous maximum appears at $\epsilon \approx 0.1$ for the 11th harmonic. For the harmonics well above the threshold, they also observed smooth decay of the yields. Instead, due to the initial velocity of the tunneling process, these harmonics exhibit a nearly Gaussian ellipticity dependence as explained by the simple man's model. Their further calculations suggested that the ellipticity dependence of the low-order harmonics can be influenced by both the alignment angle and the bond length. These results indicated for these low-order harmonics, multiphoton effects may also play an important role.

Very recently, Avanaki *et al* [109] further investigated this problem theoretically. With the help of their numerical solution to the TDSE, they revealed the origin of this phenomenon as the near threshold resonance with the π-symmetry molecule orbit. Although this abnormal phenomenon in atoms is not wide investigated in theory, we can safely conclude from the above investigations that the drop of harmonic yield with an increasing ellipticity is not smooth when some excited states of atoms are involved.

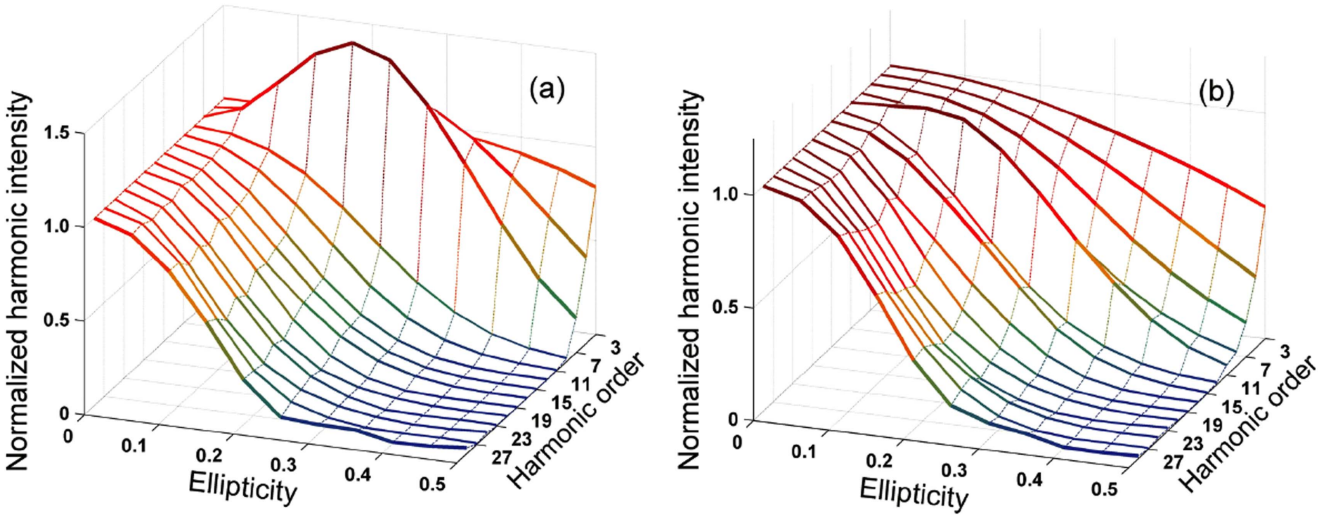

Figure 18. The normalized harmonic yields of H_2 from the 3rd to the 29th order as a function of the ellipticity for: (a) perpendicular and (b) parallel alignment, at the bond length of 2.2 a.u. Taken from [80] with permission.

The above investigations demonstrated the abnormal ellipticity dependence in molecules, which is an extension of atom BTH phenomenon in molecules. Another investigation area of the molecular BTH lies in the extension of the well studied molecular HHG to the BTH regime. Recently, the generation of circularly polarized harmonics is demonstrated in experiments with two color counter-rotating driving laser pulses [110]. Another way to generate harmonics with some degree of ellipticity is the interaction of the strong driving pulse with molecules [111]. Ellipticity of generated harmonics can also be observed in BTHs of molecules. The polarization properties of BTHs from H_2^+ were investigated recently [82, 83]. The authors found the ellipticity of BTHs depends strongly on the orientation angle and differs significantly for different harmonic orders [82]. They studied the polarization properties of BTHs from aligned molecules in linearly polarized laser fields numerically and analytically. Their results indicate that the ellipticity of low-order harmonics is closely associated with resonance effects and the symmetry axis of the molecule.

In a further investigation [83], a broad plateau for NTHs was observed in the calculated harmonic spectrum. This plateau is several orders of magnitude higher than that for high-order harmonics and shows high ellipticity at small and intermediate orientation angles. Their analysis revealed that the main contributions to the NTH plateau come from the transition of the electron from the continuum states to these two lowest bound states of the system, which are strongly coupled together by the laser field. Besides the continuum states, highly excited states also play important roles in the NTH plateau, resulting in a large phase difference between parallel and perpendicular harmonics and accordingly leads to a high ellipticity of the plateau.

Another feature of molecular harmonics is the generation of even order harmonics, which can also be observed in the NTH region. Avanaki *et al* [112] examined the harmonic generation from H_2^+ driven by an elliptically polarized pulse at both its equilibrium internuclear distance $R = 2$ a.u. and a stretched distance at $R = 7$ a.u. They observed the decrease of the harmonic yield with the increase of the ellipticity and a weaker even BTH for stretched molecules. To further explore the mechanism of the below threshold even harmonic generation in H_2^+ [81], they calculated the harmonic spectra at different internuclear distances and found that the even order harmonics are mostly observed for $R = 5$ a.u. to $R = 9$ a.u., which can be explained in the framework of Floquet theory.

On the one hand, the complicated structures of molecules can bring new features in NTHs; on the other hand, the manipulation of the molecules can reveal further understanding inside the harmonic generation process. Two years ago, Riviŕe *et al* [84] investigated the emission time of NTHs making use of the probing attosecond dynamics by chirp encoded recollisions (PACER) technique. The PACER technique was previously applied in molecules to detect the nuclear motion during the HHG process [113, 114].

Taking advantage of this method, the authors in [84] showed that the emission times of BTHs and NTHs can be reconstructed with H_2^+ molecular ion and its isotopes. The key idea of this study was that the recombination step responsible for the harmonic emission conquers the Coulomb explosion at different times, depending on the final vibrational states of the molecule. As a consequence, interferences between different vibrational channels can be observed, enabling an enhanced temporal resolution in the harmonic spectrum. In their investigations, the reconstruction of the emission times of BTHs showed that these emission times are associated with the short trajectories and the role of long trajectories cannot be clearly observed.

In figure 19, we show their calculated harmonics for different isotopes of H_2^+ molecular ion. The differences observed for different isotopes in the cutoff region have been explained by Lein [113]: since the recombination step of

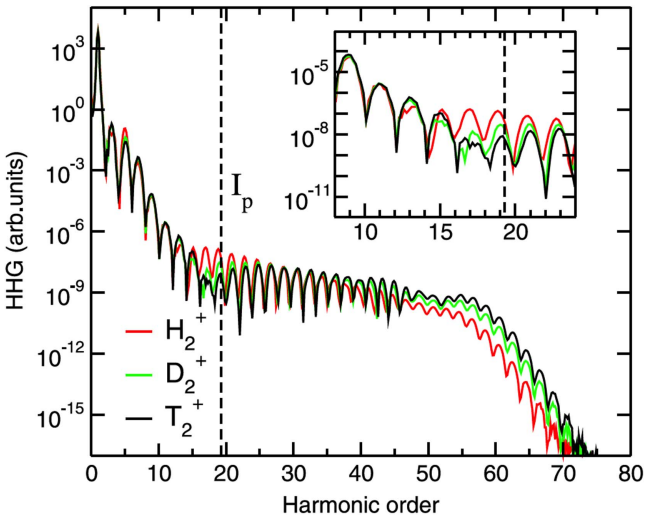

Figure 19. Comparisons of harmonic spectra for different isotopes of hydrogen molecular ions, driven by a five-cycle IR pulse with a central wavelength of 800 nm and a peak intensity of 3×10^{14} W cm^{-2}. The part near the ionization threshold is zoomed in the inset. Reprinted with permission from [84].

harmonic emission requires the system to return to its initial state, the harmonic intensity is proportional to the autocorrelation function between the wavepackets in the initial electronic and the continuum electronic states. The autocorrelation function decays faster due to the faster motion of the nuclei for the light nuclei. The fast decay suppresses the contributions of the long trajectories in the cutoff region.

However, the harmonic yield seems different in the NTH region. In this region, one can see two minima in the intensity of the harmonic peaks for the three isotopes. For H_2^+, the minima are located at the 3rd harmonic and the 13th to the 15th harmonic; for D_2^+ at the 3rd harmonic and the 17th harmonic; and for the heaviest isotope T_2^+ at the 3rd harmonic and the 17th to the 19th harmonic. The position of the minimum around the 3rd harmonic does not depend on the nuclear mass and can be explained by the fast variation of the tunneling ionization probability.

The minima at the higher harmonic orders are more pronounced than that for the 3rd harmonic. The positions of this minimum around I_p depend on the nuclear mass. This minimum can be explained by the destructive interferences between these wave packets during the recombination step and can be used to extract the emission times of the corresponding harmonics and identify the physical process responsible for the emission. For the heavy isotopes, the nuclear moves slower than the light isotopes and thus it takes longer time to form the interference minimum. The results here indicate that the heavy isotopes get the interference minimum for higher harmonic order, which means it takes a longer time for higher harmonics to recombine. This result agrees with the short trajectories in the simple man's model. This investigation indicated that the short trajectories dominate the low-order harmonics, while several previous studies in atoms stressed the role of long trajectories [29, 30].

5. Conclusions

The recent theoretical and experimental investigations on NTHs revealed that the features of these harmonics have some similarities to and drastic differences from the high-order harmonics. Due to the potential applications to use these harmonics as high repetition rate light sources and spectroscopic tools, one needs to get a more comprehensive understanding of the underlying mechanisms of NTHs, both on a single atom level and on their features after the consideration of the macroscopic effects.

The experimental studies have investigated their properties as light sources, such as the coherence, spatial distributions and wavelength range etc. The experimental investigations revealed that the quality of the low-order harmonics is as good as HHG and suggested the quantum path picture can be extended to this region. In experiments, the short and long trajectories can be separated in the far field. Further investigations indicated that the long trajectories follow the simple man's model and the short trajectories are more affected by the resonances.

The theoretical investigations have mostly focused on the underlying physics of the harmonic generation process, which reveals the electron dynamic during the interaction with strong laser fields. With the help of semi-classical methods and the time–frequency analysis, the semiclassical interpretations for the low-order harmonics have been gradually accepted. These investigations have clarified the NTH generation process in atoms as well as molecules in some degree. Since molecules have more complicated structures and degrees of freedom, the NTHs in molecules have begun to reveal more interesting features and underlying physics.

The investigation on the NTHs has also gone beyond the properties as light sources. The attention has now been focused on the dynamics of the bound electrons and the nuclear dynamics in molecules which remains an interesting topic in the strong field community. Despite of these inspiring progresses that have been made, there remain many controversial issues and unexplored topics in the low-order harmonics. The incomplete understanding is largely due to the important impacts of the Coulomb potential and the bound-state dynamics. In addition, how these new phenomena in NTHs will react to the macroscopic propagation in the medium is another important topic to be further addressed.

Acknowledgments

We cordially thank the Referees and the Member from the Editorial Board for all the kind suggestions for structuring and presenting this Topical Review during all the reviewing processes. This work is supported by National Natural Science Foundation of China (NSFC) under Grants No. 11322437 and No. 11574010 and by the National Program on Key Basic Research Project of China (973 Program) under Grant No. 2013CB922402.

References

[1] Agostini P, Fabre F, Mainfray G, Petite G and Rahman N K 1979 Free-free transitions following six-photon ionization of xenon atoms *Phys. Rev. Lett.* **42** 1127

[2] Becker W, Grasbon F, Kopold R, Milošević D, Paulus G and Walther H 2002 Above-threshold ionization: from classical features to quantum effects *Adv. At., Molec., Opt. Phys.* **48** 35

[3] Milosevic D B, Paulus G G, Bauer D and Becker W 2006 Above-threshold ionization by few-cycle pulses *J. Phys. B: At. Mol. Opt. Phys.* **39** R203

[4] Mcpherson A, Gibson G, Jara H, Johann U, Luk T S, Mcintyre I A, Boyer K and Rhodes C K 1987 Studies of multiphoton production of vacuum ultraviolet-radiation in the rare-gases *J. Opt. Soc. Am.* **4** 595

[5] Ferray M, L'Huillier A, Li X, Lompre L A, Mainfray G and Manus C 1988 Multiple-harmonic conversion of 1064-nm radiation in rare-gases *J. Phys. B: At. Mol. Opt. Phys.* **21** L31

[6] Becker W, Liu X J, Ho P J and Eberly J H 2012 Theories of photoelectron correlation in laser-driven multiple atomic ionization *Rev. Mod. Phys.* **84** 1011

[7] Frasinski L J, Codling K, Hatherly P, Barr J, Ross I N and Toner W T 1987 Femtosecond dynamics of multielectron dissociative ionization by use of a picosecond laser *Phys. Rev. Lett.* **58** 2424

[8] Zhao K, Zhang Q, Chini M, Wu Y, Wang X and Chang Z 2012 Tailoring a 67 attosecond pulse through advantageous phase-mismatch *Opt. Lett.* **37** 3891

[9] Sansone G, Poletto L and Nisoli M 2011 High-energy attosecond light sources *Nat. Photon.* **5** 656

[10] Chini M, Zhao K and Chang Z 2014 The generation, characterization and applications of broadband isolated attosecond pulses *Nat. Photon.* **8** 178

[11] Krausz F and Ivanov M 2009 Attosecond physics *Rev. Mod. Phys.* **81** 163

[12] Pazourek R, Nagele S and Burgdörfer J 2015 Attosecond chronoscopy of photoemission *Rev. Mod. Phys.* **87** 765

[13] Peng L-Y, Jiang W-C, Geng J-W, Xiong W-H and Gong Q 2015 Tracing and controlling electronic dynamics in atoms and molecules by attosecond pulses *Phys. Rep.* **575** 1

[14] Calegari F, Sansone G, Stagira S, Vozzi C and Nisoli M 2016 Advances in attosecond science *J. Phys. B: At. Mol. Opt. Phys.* **49** 062001

[15] Carman R L, Rhodes C K and Benjamin R F 1981 Observation of harmonics in the visible and ultraviolet created in CO_2-laser-produced plasmas *Phys. Rev.* A **24** 2649

[16] Teubner U and Gibbon P 2009 High-order harmonics from laser-irradiated plasma surfaces *Rev. Mod. Phys.* **81** 445

[17] Lhuillier A, Schafer K and Kulander K 1991 Theoretical aspects of intense field harmonic-generation *J. Phys. B: At. Mol. Opt. Phys.* **24** 3315

[18] Paul P M, Toma E S, Breger P, Mullot G, Auǵe F, Balcou P, Muller H G and Agostini P 2001 Observation of a train of attosecond pulses from high harmonic generation *Science* **292** 1689

[19] Hentschel M, Kienberger R, Spielmann C, Reider G, Milosevic N, Brabec T, Corkum P, Heinzmann U, Drescher M and Krausz F 2001 Attosecond metrology *Nature* **414** 509

[20] Drescher M, Hentschel M, Kienberger R, Tempea G, Spielmann C, Reider G, Corkum P and Krausz F 2001 X-ray pulses approaching the attosecond frontier *Science* **291** 1923

[21] Popmintchev T, Chen M-C, Arpin P, Murnane M M and Kapteyn H C 2010 The attosecond nonlinear optics of bright coherent x-ray generation *Nat. Photon.* **4** 822

[22] Popmintchev T *et al* 2012 Bright coherent ultrahigh harmonics in the kev x-ray regime from mid-infrared femtosecond lasers *Science* **336** 12878

[23] Burnett N, Kan C and Corkum P 1995 Ellipticity and polarization effects in harmonic generation in ionizing neon *Phys. Rev.* A **51** R3418

[24] Miyazaki K and Takada H 1995 High-order harmonic-generation in the tunneling regime *Phys. Rev.* A **52** 3007

[25] Kakehata M, Takada H, Yumoto H and Miyazaki K 1997 Anomalous ellipticity dependence of high-order harmonic generation *Phys. Rev.* A **55** R861

[26] Ivanov M, Brabec T and Burnett N 1996 Coulomb corrections and polarization effects in high-intensity high-harmonic emission *Phys. Rev.* A **54** 742

[27] Gohle C, Udem T, Herrmann M, Rauschenberger J, Holzwarth R, Schuessler H, Krausz F and Hansch T 2005 A frequency comb in the extreme ultraviolet *Nature* **436** 234

[28] Cingoz A, Yost D C, Allison T K, Ruehl A, Fermann M E, Hartl I and Ye J 2012 Direct frequency comb spectroscopy in the extreme ultraviolet *Nature* **482** 68

[29] Yost D C, Schibli T R, Ye J, Tate J L, Hostetter J, Gaarde M B and Schafer K J 2009 Vacuum-ultraviolet frequency combs from below-threshold harmonics *Nat. Phys.* **5** 815

[30] Power E P, March A M, Catoire F, Sistrunk E, Krushelnick K, Agostini P and DiMauro L F 2010 XFROG phase measurement of threshold harmonics in a Keldysh-scaled system *Nat. Photon.* **4** 352

[31] Soifer H, Botheron P, Shafir D, Diner A, Raz O, Bruner B D, Mairesse Y, Pons B and Dudovich N 2010 Near-threshold high-order harmonic spectroscopy with aligned molecules *Phys. Rev. Lett.* **105** 143904

[32] Chini M *et al* 2014 Coherent phase-matched VUV generation by field-controlled bound states *Nat. Photon.* **8** 437

[33] Hassan M T *et al* 2016 Optical attosecond pulses and tracking the nonlinear response of bound electrons *Nature* **530** 66

[34] Hammond T J, Mills A K and Jones D J 2011 Near-threshold harmonics from a femtosecond enhancement cavity-based EUV source: effects of multiple quantum pathways on spatial profile and yield *Opt. Express* **19** 24871

[35] Bernhardt B *et al* 2012 Vacuum ultraviolet frequency combs generated by a femtosecond enhancement cavity in the visible *Opt. Lett.* **37** 503

[36] Burnett K, Reed V, Cooper J and Knight P 1992 Calculation of the background emitted during high-harmonic generation *Phys. Rev.* A **45** 3347

[37] Lewenstein M, Balcou P, Ivanov M, Lhuillier A and Corkum P 1994 Theory of high-harmonic generation by low-frequency laser fields *Phys. Rev.* A **49** 2117

[38] Morishita T, Le A-T, Chen Z and Lin C D 2008 Accurate retrieval of structural information from laser-induced photoelectron and high-order harmonic spectra by few-cycle laser pulses *Phys. Rev. Lett.* **100** 013903

[39] Le A-T, Lucchese R R, Tonzani S, Morishita T and Lin C D 2009 Quantitative rescattering theory for high-order harmonic generation from molecules *Phys. Rev.* A **80** 013401

[40] Lin C D, Le A-T, Chen Z, Morishita T and Lucchese R 2010 Strong-field rescattering physicsself-imaging of a molecule by its own electrons *J. Phys. B: At. Mol. Opt. Phys.* **43** 122001

[41] Schafer K J, Yang B, Dimauro L F and Kulander K C 1993 Above threshold ionization beyond the high harmonic cutoff *Phys. Rev. Lett.* **70** 1599

[42] Corkum P B 1993 Plasma perspective on strong-field multiphoton ionization *Phys. Rev. Lett.* **71** 1994

[43] Paulus G G, Becker W, Nicklich W and Walther H 1994 Rescattering effects in above-threshold ionization—a classical-model *J. Phys. B: At. Mol. Opt. Phys.* **27** L703

[44] Spott A, Becker A and Jaron-Becker A 2015 Transition from perturbative to nonperturbative interaction in low-order-harmonic generation *Phys. Rev.* A **91** 023402
[45] Xiong W-H, Geng J-W, Tang J-Y, Peng L-Y and Gong Q 2014 Mechanisms of below-threshold harmonic generation in atoms *Phys. Rev. Lett.* **112** 233001
[46] Hostetter J A, Tate J L, Schafer K J and Gaarde M B 2010 Semiclassical approaches to below-threshold harmonics *Phys. Rev.* A **82** 023401
[47] Xiong W-H, Geng J-W, Gong Q and Peng L-Y 2015 Half-cycle cutoff in near-threshold harmonic generation *New J. Phys.* **17** 123020
[48] Li P-C, Sheu Y-L, Laughlin C and Chu S-I 2014 Role of laser-driven electron-multirescattering in resonance-enhanced below-threshold harmonic generation in He atoms *Phys. Rev.* A **90** 041401(R)
[49] Li P-C, Sheu Y-L, Laughlin C and Chu S-I 2015 Dynamical origin of near- and below-threshold harmonic generation of Cs in an intense mid-infrared laser field *Nat. Commun.* **6** 7178
[50] Muller H G 1999 An efficient propagation scheme for the time-dependent Schrödinger equation in the velocity gauge *Laser Phys.* **9** 138
[51] Bauer D and Koval P 2006 QPROP: a Schrodinger-solver for intense laser-atom interaction *Comput. Phys. Commun.* **174** 396
[52] Smyth E, Parker J and Taylor K 1998 Numerical integration of the time-dependent Schrodinger equation for laser-driven helium *Comput. Phys. Commun.* **114** 1
[53] Antoine P, Piraux B and Maquet A 1995 Time profile of harmonics generated by a single atom in a strong electromagnetic field *Phys. Rev.* A **51** R1750
[54] Tong X-M and Chu S-I 2000 Probing the spectral and temporal structures of high-order harmonic generation in intense laser pulses *Phys. Rev.* A **61** 021802
[55] Figueira de Morisson Faria C and Rotter I 2002 High-order harmonic generation in a driven two-level atom: periodic level crossings and three-step processes *Phys. Rev.* A **66** 013402
[56] Tate J, Auguste T, Muller H G, Salieres P, Agostini P and DiMauro L F 2007 Scaling of wave-packet dynamics in an intense midinfrared field *Phys. Rev. Lett.* **98** 013901
[57] Salieres P *et al* 2001 Feynman's path-integral approach for intense-laser-atom interactions *Science* **292** 902
[58] Kopold R, Becker W and Kleber M 2000 Quantum path analysis of high-order above-threshold ionization *Opt. Commun.* **179** 39
[59] Zair A *et al* 2008 Quantum path interferences in high-order harmonic generation *Phys. Rev. Lett.* **100** 143902
[60] Brabec T, Ivanov M and Corkum P 1996 Coulomb focusing in intense field atomic processes *Phys. Rev.* A **54** R2551
[61] Chen J, Liu J, Fu L and Zheng W 2001 Interpretation of momentum distribution of recoil ions from laser-induced nonsequential double ionization by semiclassical rescattering model *Phys. Rev.* A **63** 011404
[62] Yudin G and Ivanov M 2001 Physics of correlated double ionization of atoms in intense laser fields: quasistatic tunneling limit *Phys. Rev.* A **63** 033404
[63] Ye D F, Liu X and Liu J 2008 Classical trajectory diagnosis of a fingerlike pattern in the correlated electron momentum distribution in strong field double ionization of helium *Phys. Rev. Lett.* **101** 233003
[64] Hu B, Liu J and Chen S 1997 Plateau in above-threshold-ionization spectra and chaotic behavior in rescattering processes *Phys. Lett.* A **236** 533
[65] Shvetsov-Shilovski N I, Dimitrovski D and Madsen L B 2012 Ionization in elliptically polarized pulses: multielectron polarization effects and asymmetry of photoelectron momentum distributions *Phys. Rev.* A **85** 023428
[66] Ammosov M V, Delone N B and Krainov V P 1986 Tunnel ionization of complex atoms and of atomic ions in an alternating electromagnetic field *Sov. Phys—JETP* **64** 1191
[67] Lambert G *et al* 2015 Spatial properties of odd and even low order harmonics generated in gas *Sci. Rep.* **5** 7786
[68] Brizuela F, Heyl C M, Rudawski P, Kroon D, Rading L, Dahlstrom J M, Mauritsson J, Johnsson P, Arnold C L and L'Huillier A 2013 Efficient high-order harmonic generation boosted by below-threshold harmonics *Sci. Rep.* **3** 1410
[69] Liang Y, Ammosov M and Chin S 1994 High-order harmonic-generation in argon by ellipticity polarized picosecond dye-laser pulses *J. Phys. B: At. Mol. Opt. Phys.* **27** 1269
[70] Lein M, Hay N, Velotta R, Marangos J and Knight P 2002 Role of the intramolecular phase in high-harmonic generation *Phys. Rev. Lett.* **88** 183903
[71] Vozzi C *et al* 2005 Controlling two-center interference in molecular high harmonic generation *Phys. Rev. Lett.* **95** 153902
[72] Kanai T, Minemoto S and Sakai H 2005 Quantum interference during high-order harmonic generation from aligned molecules *Nature* **435** 470
[73] Bian X-B and Bandrauk A D 2010 Multichannel molecular high-order harmonic generation from asymmetric diatomic molecules *Phys. Rev. Lett.* **105** 093903
[74] Chen Y J, Fu L B and Liu J 2013 Asymmetric molecular imaging through decoding odd–even high-order harmonics *Phys. Rev. Lett.* **111** 073902
[75] Kanai T, Minemoto S and Sakai H 2007 Ellipticity dependence of high-order harmonic generation from aligned molecules *Phys. Rev. Lett.* **98** 053002
[76] Balcou P, Dederichs A, Gaarde M and L'Huillier A 1999 Quantum-path analysis and phase matching of high-order harmonic generation and high-order frequency mixing processes in strong laser fields *J. Phys. B: At. Mol. Opt. Phys.* **32** 2973
[77] Sola I *et al* 2006 Controlling attosecond electron dynamics by phase-stabilized polarization gating *Nat. Phys.* **2** 319
[78] Camp S, Schafer K J and Gaarde M B 2015 Interplay between resonant enhancement and quantum path dynamics in harmonic generation in helium *Phys. Rev.* A **92** 013404
[79] Xiong W-H, Xiao X-R, Peng L-Y and Gong Q 2016 Correspondence of below threshold harmonic generation and frustrated tunnelling ionization *Phys. Rev.* A **94** 013417
[80] Yang H, Liu P, Li R and Xu Z 2013 Ellipticity dependence of the near-threshold harmonics of H_2 in an elliptical strong laser field *Opt. Express* **21** 28676
[81] Avanaki K N, Telnov D A, Jooya H Z and Chu S-I 2015 Generation of below-threshold even harmonics by a stretched H_2^+ molecular ion in intense linearly and circularly polarized laser fields *Phys. Rev.* A **92** 063811
[82] Dong F, Tian Y, Yu S, Wang S, Yang S and Chen Y 2015 Polarization properties of below-threshold harmonics from aligned molecules H_2^+ in linearly polarized laser fields *Opt. Express* **23** 18106
[83] Li W, Dong F, Yu S, Wang S, Yang S and Chen Y 2015 Ellipticity of near-threshold harmonics from stretched molecules *Opt. Express* **23** 31010
[84] Riviere P, Morales F, Richter M, Medisauskas L, Smirnova O and Martin F 2014 Time reconstruction of harmonic emission in molecules near the ionization threshold *J. Phys. B: At. Mol. Opt. Phys.* **47** 241001
[85] Henkel J, Witting T, Fabris D, Lein M, Knight P L, Tisch J W G and Marangos J P 2013 Prediction of attosecond light pulses in the VUV range in a high-order-harmonic-generation regime *Phys. Rev.* A **87** 043818
[86] Frolov M V, Manakov N L and Starace A F 2008 Wavelength scaling of high-harmonic yield: threshold phenomena and

bound state symmetry dependence *Phys. Rev. Lett.* **100** 173001
[87] Frolov M V, Manakov N L, Sarantseva T S, Emelin M Y, Ryabikin M Y and Starace A F 2009 Analytic description of the high-energy plateau in harmonic generation by atoms: can the harmonic power increase with increasing laser wavelengths? *Phys. Rev. Lett.* **102** 243901
[88] Ishikawa K L, Schiessl K, Persson E and Burgdoerfer J 2009 Fine-scale oscillations in the wavelength and intensity dependence of high-order harmonic generation: connection with channel closings *Phys. Rev.* A **79** 033411
[89] Perez-Hernandez J A, Roso L and Plaja L 2009 Harmonic generation beyond the strong-field approximation: the physics behind the short-wave-infrared scaling laws *Opt. Express* **17** 9891
[90] Schiessl K, Ishikawa K L, Persson E and Burgdoerfer J 2007 Quantum path interference in the wavelength dependence of high-harmonic generation *Phys. Rev. Lett.* **99** 253903
[91] Lan P, Takahashi E J and Midorikawa K 2010 Wavelength scaling of efficient high-order harmonic generation by two-color infrared laser fields *Phys. Rev.* A **81** 061802
[92] Xu H, Xiong H, Zeng B, Chu W, Fu Y, Yao J, Chen J, Liu X, Cheng Y and Xu Z 2010 Wavelength scaling of elliptical-polarization dependence of high-order harmonic generation *Opt. Lett.* **35** 472
[93] Yavuz I, Altun Z and Topcu T 2012 Wavelength scaling of high-order-harmonic-generation efficiency by few-cycle laser pulses: influence of carrier-envelope phase *Phys. Rev.* A **86** 043836
[94] Austin D R and Biegert J 2012 Strong-field approximation for the wavelength scaling of high-harmonic generation *Phys. Rev.* A **86** 023813
[95] Le A-T, Wei H, Jin C, Tuoc V N, Morishita T and Lin C D 2014 Universality of returning electron wave packet in high-order harmonic generation with midinfrared laser pulses *Phys. Rev. Lett.* **113** 033001
[96] Frolov M V, Manakov N L, Xiong W-H, Peng L-Y, Burgdörfer J and Starace A F 2015 Comment on 'Universality of returning electron wave packet in high-order harmonic generation with midinfrared laser pulses' *Phys. Rev. Lett.* **114** 069301
[97] Shiner A D, Trallero-Herrero C, Kajumba N, Bandulet H C, Comtois D, Legare F, Giguere M, Kieffer J-C, Corkum P B and Villeneuve D M 2009 Wavelength scaling of high harmonic generation efficiency *Phys. Rev. Lett.* **103** 073902
[98] Lai C-J, Cirmi G, Hong K-H, Moses J, Huang S-W, Granados E, Keathley P, Bhardwaj S and Kärtner F X 2013 Wavelength scaling of high harmonic generation close to the multiphoton ionization regime *Phys. Rev. Lett.* **111** 073901
[99] Milosevic D and Becker W 2002 Role of long quantum orbits in high-order harmonic generation *Phys. Rev.* A **66** 063417
[100] Gaarde M and Schafer K 2000 Calculations of resonant, multiphoton population transfer in potassium atoms at long wavelengths *Phys. Rev.* A **62** 053411
[101] Gaarde M and Schafer K 2001 Enhancement of many high-order harmonics via a single multiphoton resonance *Phys. Rev.* A **64** 013820
[102] Wassaf J, Veniard V, Taieb R and Maquet A 2003 Roles of resonances and recollisions in strong-field atomic phenomena: above-threshold ionization *Phys. Rev.* A **67** 053405
[103] Taieb R, Veniard V, Wassaf J and Maquet A 2003 Roles of resonances and recollisions in strong-field atomic phenomena: II. High-order harmonic generation *Phys. Rev.* A **68** 033403
[104] Haworth C A, Chipperfield L E, Robinson J S, Knight P L, Marangos J P and Tisch J W G 2007 Half-cycle cutoffs in harmonic spectra and robust carrier-envelope phase retrieval *Nat. Phys* **3** 52–7
[105] Ishii N, Kaneshima K, Kitano K, Kanai T, Watanabe S and Itatani J 2014 Carrier-envelope phase-dependent high harmonic generation in the water window using few-cycle infrared pulses *Nat. Commun.* **5** 3331
[106] Nubbemeyer T, Gorling K, Saenz A, Eichmann U and Sandner W 2008 Strong-field tunneling without ionization *Phys. Rev. Lett.* **101** 233001
[107] Landsman A S, Pfeiffer A N, Hofmann C, Smolarski M, Cirelli C and Keller U 2013 Rydberg state creation by tunnel ionization *New J. Phys.* **15** 013001
[108] Liu H *et al* 2012 Low yield of near-zero-momentum electrons and partial atomic stabilization in strong-field tunneling ionization *Phys. Rev. Lett.* **109** 093001
[109] Avanaki K N, Telnov D A and Chu S-I 2016 Exploration of the origin of anomalous dependence for near-threshold harmonics in H_2^+ on the ellipticity of driving laser fields *J. Phys. B: At. Mol. Opt. Phys.* **49** 114002
[110] Kfir O *et al* 2015 Generation of bright phase-matched circularly-polarized extreme ultraviolet high harmonics *Nat. Photon,* **9** 99
[111] Yuan K-J and Bandrauk A D 2011 Generation of circularly polarized attosecond pulses by intense ultrashort laser pulses from extended asymmetric molecular ions *Phys. Rev.* A **84** 023410
[112] Avanaki K N, Telnov D A and Chu S-I 2014 Above- and below-threshold high-order-harmonic generation of H_2^+ in intense elliptically polarized laser fields *Phys. Rev.* A **90** 033425
[113] Lein M 2005 Attosecond probing of vibrational dynamics with high-harmonic generation *Phys. Rev. Lett.* **94** 053004
[114] Baker S, Robinson J, Haworth C, Teng H, Smith R, Chirila C, Lein M, Tisch J and Marangos J 2006 Probing proton dynamics in molecules on an attosecond time scale *Science* **312** 424